Resurgent sodium current promotes action potential firing in the avian auditory brainstem

Hui Hong[1] (iD), Ting Lu[1] (iD), Xiaoyu Wang[4,5], Yuan Wang[4,5] and Jason Tait Sanchez[1,2,3] (iD)

[1] *Roxelyn and Richard Pepper Department of Communication Sciences and Disorders, Northwestern University, Evanston, IL 60208, USA*
[2] *Department of Neurobiology, Northwestern University, Evanston, IL 60208, USA*
[3] *The Hugh Knowles Hearing Research Center, Northwestern University, Evanston, IL 60208, USA*
[4] *Department of Biomedical Sciences, Florida State University, Tallahassee, FL 32306, USA*
[5] *Program in Neuroscience Florida State University College of Medicine, Florida State University, Tallahassee, FL 32306, USA*

Edited by: Ian Forsythe & Walter Marcotti

The Journal of Physiology

Key points

- Auditory brainstem neurons of all vertebrates fire phase-locked action potentials (APs) at high rates with remarkable fidelity, a process controlled by specialized anatomical and biophysical properties.
- This is especially true in the avian nucleus magnocellularis (NM) – the analogue of the mammalian anteroventral cochlear nucleus.
- In addition to high voltage-activated potassium (K_{HVA}) channels, we report, using whole cell physiology and modelling, that resurgent sodium current (I_{NaR}) of sodium channels (Na_V) is equally important and operates synergistically with K_{HVA} channels to enable rapid AP firing in NM.
- Anatomically, we detected strong $Na_V 1.6$ expression near hearing maturation, which was less distinct during hearing development despite functional evidence of I_{NaR}, suggesting that multiple Na_V channel subtypes may contribute to I_{NaR}.
- We conclude that I_{NaR} plays an important role in regulating rapid AP firing for NM neurons, a property that may be evolutionarily conserved for functions related to similar avian and mammalian hearing.

Abstract Auditory brainstem neurons are functionally primed to fire action potentials (APs) at markedly high rates in order to rapidly encode the acoustic information of sound. This specialization is critical for survival and the comprehension of behaviourally relevant communication functions, including sound localization and distinguishing speech from noise. Here, we investigated underlying ion channel mechanisms essential for high-rate AP firing in neurons of the chicken nucleus magnocellularis (NM) – the avian analogue of bushy cells of the mammalian anteroventral cochlear nucleus. In addition to the established function of high voltage-activated potassium channels, we found that resurgent sodium current (I_{NaR}) plays a role in regulating rapid firing activity of late-developing (embryonic (E) days 19–21) NM neurons. I_{NaR} of late-developing NM neurons showed similar properties to mammalian neurons in that its unique mechanism of an 'open channel block state' facilitated the recovery and increased the availability of sodium (Na_V) channels after depolarization. Using a computational model of NM neurons, we demonstrated that removal of I_{NaR} reduced high-rate AP firing. We found weak I_{NaR} during a prehearing period (E11–12), which transformed to resemble late-developing I_{NaR} properties around hearing onset (E14–16). Anatomically, we detected strong $Na_V 1.6$ expression near maturation, which became increasingly less distinct at hearing onset and prehearing periods, suggesting that multiple Na_V channel subtypes may contribute to I_{NaR} during development. We conclude that I_{NaR} plays an important role in regulating rapid AP firing for NM neurons, a property

that may be evolutionarily conserved for functions related to similar avian and mammalian hearing.

Corresponding author J. T. Sanchez: Roxelyn and Richard Pepper Department of Communication Sciences and Disorders, Northwestern University, Frances Searle Building, 2240 Campus Drive, Evanston, IL 60208, USA. Email: jason.sanchez@northwestern.edu

Introduction

Voltage-dependent sodium (Na_V) channels play a critical role in generation of action potentials (APs), the firing pattern of which is fundamental for information processing in the nervous system (Eijkelkamp *et al.* 2012). A unique property of some Na_V channels is a resurgent sodium current (I_{NaR}) (Raman & Bean, 1997). I_{NaR} is the result of a voltage-dependent open channel block of the Na_V α-subunit by an intracellular particle that competes with the classic inactivation gate (i.e. the cytoplasmic linker between the III and IV domains of the α-subunit) during depolarization. Channels that are in the 'blocked' state, but not the 'classic-inactivated' state, generate I_{NaR} during AP repolarization because the open channel blocker loses affinity for the α-subunit at repolarized membrane potentials. As a result, I_{NaR} provides a small depolarizing drive to the membrane near the AP threshold – a property that promotes repetitive neuronal firing. In addition, activation of the open channel blocker facilitates the recovery of Na_V channels after depolarization and increases Na_V channel availability by competing against classic inactivation (Raman & Bean, 2001). This specific blocker has been identified as the β4-subunit in cerebellar Purkinje cells (Grieco *et al.* 2005; Aman *et al.* 2009), whereas multiple α-subunits (e.g. Na_V1.2, 1.5, 1.6 and 1.7) have been shown to be capable of carrying I_{NaR} (Rush *et al.* 2005; Jarecki *et al.* 2010). As a result of unique features of the open channel blocker, studies show that I_{NaR} plays an important role in promoting high rates of AP firing in numerous mammalian neurons, underlying their highly specialized information processing patterns (Lewis & Raman, 2014).

In the auditory brainstem of all vertebrates, neurons are known for their remarkable ability to fire APs at high rates (Oertel, 1997). This specialization is important for encoding sound in an ultrafast and temporally precise manner, properties essential for survival and comprehension of behaviourally relevant communication functions, including sound localization and signal extraction in complex listening environments (Shannon *et al.* 1995; Anderson *et al.* 2010; Grothe *et al.* 2010). An exemplar of this ability is well studied in the avian auditory brainstem. Neurons in nucleus magnocellularis (NM) – the avian analogue of bushy cells of the mammalian anteroventral cochlear nucleus – are able to phase-lock to inputs up to 1000 Hz with high fidelity, as demonstrated by single-unit recordings from barn owls (Koppl & Carr, 1997). Similarly, in the mammalian auditory brainstem, the calyx of Held is a pivotal synapse involved in the microsecond precision of sound localization computations. Here, fast Na_V channel kinetics (Leao *et al.* 2005) and abundant expression of high voltage-activated potassium channels (K_{HVA}) (Wang *et al.* 1998) along with I_{NaR} present at both pre- and postsynaptic sites (Leao *et al.* 2006; Kim *et al.* 2010) promote high rates of AP firing. Based on the aforementioned properties of I_{NaR} in mammals, as well as the established and shared functional phenotypes between species (Carr & Soares, 2002), we hypothesized that this unique current also plays an important role in shaping the fast firing pattern observed for avian NM neurons.

In this study we tested whether NM neurons present with I_{NaR}. By investigating the function of I_{NaR} in AP firing rates of chicken NM neurons both experimentally and computationally, we found that NM neurons have robust I_{NaR} that significantly increases Na_V availability immediately after depolarization and facilitates Na_V channel recovery. Removal of I_{NaR} in a model NM neuron undermines its ability to fire at high rates. We also examined the maturation of I_{NaR} relative to hearing onset and the potential Na_V channel subtype that carries this current in developing NM using immunocytochemistry. We conclude that I_{NaR} plays an important role in regulating rapid AP firing for NM neurons, a property that may be evolutionarily conserved for functions related to similar avian and mammalian hearing.

Methods

In vitro electrophysiology in brainstem slices

Slice preparation. All animal procedures were approved by the Northwestern University and Florida State University Institutional Animal Care and Use Committees and conducted in accordance with the National Institutes of Health Guide for the Care and Use of Laboratory Animals. Acute brainstem slices were prepared from 96 White Leghorn chicken (*Gallus gallus domesticus*) embryos of either sex as previously described (Sanchez *et al.* 2011; Hong *et al.* 2016). Briefly, embryos were rapidly decapitated and the brain was dissected from the skull to isolate the brainstem region of interest. This procedure is consistent with the recommendation from the Panel on Euthanasia of the American Veterinary Medical

Association and is appropriate for the species, stages of development and size of the embryos. For electrophysiological experiments, eggs were obtained from Sunnyside Farms, Inc. (Beaver Dam, WI, USA) and incubated in the central auditory physiology laboratory at Northwestern University. For immunocytochemical experiments, eggs were obtained from Charles River Laboratories (Wilmington, MA, USA) and incubated in a Florida State University vivarium. The authors understand and conform to the principles and regulations described by *The Journal of Physiology* (Grundy, 2015).

To study the stimulus frequency–firing pattern of NM neurons and the properties and function of I_{NaR}, brainstem slices were taken from chickens at embryonic days (E) 19–21. Frequency-firing pattern is defined as the calculated firing probability (see below) of APs as a function of stimulus frequency. At this age range, near-mature hearing ability is established (Saunders *et al.* 1973; Rebillard & Rubel, 1981; Jones *et al.* 2006) and NM neurons have obtained mature-like morphology and physiology (Jhaveri & Morest, 1982*b*). To study the development of I_{NaR}, along with the development of frequency–firing pattern, chickens at the age of E11–12 and E14–16 were included in the current study, corresponding to before and during hearing onset, respectively, while chickens at E19–21 were considered as after hearing onset (Jones *et al.* 2006). The brainstem was dissected and isolated in ice-cold (~0°C) oxygenated low-Ca^{2+}, high-Mg^{2+} modified artificial cerebral spinal fluid (ACSF) containing the following (in mM): 130 NaCl, 2.5 KCl, 1.25 NaH_2PO_4, 26 $NaHCO_3$, 3 $MgCl_2$, 1 $CaCl_2$ and 10 glucose. ACSF was continuously bubbled with a mixture of 95% O_2–5% CO_2 (pH 7.4, osmolarity 295–310 mosmol l^{-1}). The brainstem was blocked coronally, affixed to the stage of a vibrating blade microtome slicing chamber (Ted Pella, Inc., Redding, CA) and submerged in ice-cold ACSF. Bilaterally symmetrical coronal slices were made (200–300 μm thick) and approximately three to seven slices (depending on age) containing NM were taken from caudal to rostral, roughly representing the low-to-high frequency regions, respectively. All neurons reported here were obtained from the rostral one-half of the entire nucleus, roughly representing the mid- to high-frequency regions of NM.

Slices were collected in a custom holding chamber and allowed to equilibrate for 1 h at room temperature in normal ACSF containing the following (in mM): 130 NaCl, 2.5 KCl, 1.25 NaH_2PO_4, 26 $NaHCO_3$, 1 $MgCl_2$, 3 $CaCl_2$ and 10 glucose. Normal ACSF was continuously bubbled with a mixture of 95% O_2–5% CO_2 (pH 7.4, osmolarity 295–310 mosmol l^{-1}). Slices were transferred to a recording chamber mounted on an Olympus BX51W1 (Center Valley, PA, USA) microscope for electrophysiological experiments. The microscope was equipped with a CCD camera, ×60 water-immersion objective and infrared differential interference contrast optics. The recording chamber was superfused continuously with a motorized pump (Welco, Tokyo, Japan) at room temperature (monitored continuously with a bath emerged thermometer at ~24°C, Warner Instruments, Hamden, CT, USA) in oxygenated normal ACSF at a rate of 1.5–2 ml min^{-1}.

Whole cell electrophysiology. Voltage-clamp and current-clamp experiments were performed using an Axon Multiclamp 700B amplifier (Molecular Devices, Sunnyvale, CA, USA). Patch pipettes were pulled to a tip diameter of 1–2 μm using a P-97 Flaming–Brown micropipette puller (Sutter Instrument, Novato, CA, USA) and had resistances ranging from 3 to 6 MΩ. For voltage-clamp experiments of isolated Na_V currents, the internal solution was caesium-based and contained the following (in mM): 150 CsCl, 10 NaCl, 0.2 EGTA and 10 HEPES, pH adjusted to 7.3–7.4 with CsOH. The Cs^+-based internal solution was used to block K_V currents and reduce space-clamp issues. The junction potential was ~−3 mV. Series resistance was compensated for by ~80% in all voltage-clamp recordings. For current-clamp experiments, the internal solution was potassium-based and contained the following (in mM): 105 potassium gluconate, 35 KCl, 1 $MgCl_2$, 10 HEPES-K, 5 EGTA, 4 4-Mg_2ATP, and 0.3 4-$Tris_2$GTP, pH adjusted to 7.3–7.4 with KOH. The junction potential was ~−10 mV. Data in both voltage clamp and current clamp experiments were not corrected for junction potentials.

Pipettes were visually guided to NM and neurons were identified and distinguished from surrounding tissue based on cell morphology, known structure and location of the nucleus within the slice. After a gigaohm seal was attained, membrane patches were ruptured and neurons were first held in the voltage clamp mode of the whole-cell configuration. A small hyperpolarizing (−1 mV, 30 ms) voltage command was presented to monitor whole-cell parameters (i.e. cell membrane capacitance, series resistance and input resistance). NM neurons were included in the data analysis only if they had series resistances <15 MΩ. Raw data were low-pass filtered at 5 kHz and digitized at 50 kHz using a Digidata 1440A (Molecular Devices).

All experiments were conducted in the presence of the $GABA_A$ receptor antagonist picrotoxin (100 μM). Synaptic glutamate transmission was continuously blocked using DL-2-amino-5-phosphonopentanoic acid (DL-APV, 100 μM, an NMDA receptor antagonist) and 6-cyano-7-nitroquinoxaline-2,3-dione (CNQX, 20 μM, an AMPA receptor antagonist). In current-clamp experiments, tetraethylammonium (TEA, 1 mM) was used to block K_V3-containing channels. Current commands of square pulse trains (duration 1 s) were injected into the soma of E19–21 NM neurons before and during TEA

application. The current strength was 1 nA and individual square pulse width was 2 ms. Square pulse trains were applied at varying frequencies: 50, 100, 150, 200, 250 and 300 Hz. In order to profile the frequency–firing pattern for NM neurons, firing probability per square pulse (for simplicity, 'firing probability') was calculated as the number of APs divided by the total number of square pulses and plotted as a function of stimulus frequency. To study the development of frequency–firing pattern, the same current commands of square pulse trains were used for NM neurons at E14–16. For NM neurons at E11–12, however, individual square pulse width was extended to 5 ms, because neurons at this age are presented with significantly wider AP half-width (average = 4.6 ms) than the other two age groups (Hong *et al.* 2016). In addition, square pulse trains were applied at different frequencies: 10, 30, 50, 70, 100, 120 and 150 Hz.

In voltage-clamp experiments, isolated Na_V currents were recorded with bath application of TEA (3 mM), 4-AP (30 μM) and $CdCl_2$ (0.2 mM) to block potassium and calcium channels. Classic voltage-clamp protocols to elicit I_{NaR} were used for NM neurons (Raman & Bean, 1997; see Results). Briefly, repolarizations at membrane voltages from −70 to 0 mV (in a step of 5 mV) were applied after a depolarizing conditioning step. Three levels of conditioning step were used, +30, 0 and −30 mV, along with two durations, 10 and 100 ms. I_{NaR} properties were characterized separately under these six experimental conditions. Afterwards, tetrodotoxin (TTX, 1 μM) was bath applied and the same voltage-clamp protocols were repeated during TTX application. Data reported in this study were obtained by subtracting the TTX-insensitive current traces from the control traces. Capacitive currents generated during voltage-clamp recordings were blanked or reduced offline.

Data analysis. Recording protocols were written and run using Clampex acquisition and Clampfit analysis software (v. 10.3; Molecular Devices). Statistical analyses and graphing protocols were performed using Prism (v. 7.0b; GraphPad Software, La Jolla, CA, USA) and MATLAB (v. R2014b; The MathWorks, Natick, MA, USA) software. Student's *t* test or analysis of variance (ANOVA) with *post hoc* Bonferroni adjusted *t* test was used to determine significance. The standard for significant differences was defined as $P < 0.05$. Numerical values in the text are reported as means ± standard deviation (SD). Numerical values in Table 3 are reported as means ± standard error of the mean (SEM). Error bars in all figures represent SEM.

Reagents. All bath-applied drugs except for TTX were allowed to perfuse through the recording chamber for ~10 min before subsequent recordings. TTX application was allowed for 3–5 min before subsequent recordings. DL-APV, CNQX and all other salts and chemicals were

Table 1. Single compartment model

Parameter	Value
Axial resistance	50 Ω cm
Temperature	24°C
E_{Na}	44 mV
E_K	−80 mV
Length	20 μm
Diameter	20 μm
g_{Leak}	0.002 S cm^{-2}
g_{NaV}	0.025 S cm^{-2}
g_{KLVA}	0.0069 S cm^{-2}
g_{KHVA}	0.004 S cm^{-2}

obtained from Sigma-Aldrich (St Louis, MO, USA). Picrotoxin was obtained from Tocris Bioscience (Ellisville, MO, USA). TTX was obtained from Alomone Labs (Jerusalem, Israel). TEA was obtained from VWR (Radnor, PA, USA).

Computational modelling

Based on NM models previously described in detail elsewhere (Howard & Rubel, 2010; Lu *et al.* 2017), a single-compartment computational model was constructed using NEURON 7.1 (Table 1) (Hines & Carnevale, 1997). This model contains currents mediated by low and high voltage-activated potassium channels (K_{LVA} and K_{HVA}, respectively), Na_V and passive leak channels. Modelling schemes were identical to those described in Lu *et al.* (2017) for all membrane currents except for Na_V currents (Table 2). The Hodgkin–Huxley style formalism, previously employed to model Na_V current, was replaced with a Markovian 13-state Na_V-channel model, which generates the transient (I_{NaT}), persistent (I_{NaP}) and resurgent (I_{NaR}) current components simultaneously (Fig. 1) (Khaliq *et al.* 2003). We adopted a modified version described previously (Akemann & Knopfel, 2006), which includes the Q_{10} parameter to adjust the Na_V current to match the experimental recording temperature of 24°C. Q_{10} is a measure of the degree to which a biological process depends on temperature. It is defined as the ratio between the rate of a biological process at two temperatures separated by 10°C. In the context of ion channels, it can be applied to the temperature dependence of the rate of channel opening and closing and to the dependence of maximum channel conductance on temperature.

To remove the I_{NaR} component, the rate constant for the O→OB transition, ε, was set to zero. This resulted in considerable slowing of I_{NaT} decay (see Fig. 6*B*, blue trace). To modify I_{NaR} without affecting I_{NaT} and I_{NaP}, we applied the method described previously (Magistretti *et al.* 2006). Kinetic constants were modified as follows: ε was set to 0; O_{on} and O_{off} were increased to 2.15 ms^{-1} and

Table 2. Model parameters

Parameter	Value
I_{NaV}, Markovian model	
α	$150\exp(V/20)$ ms^{-1}
β	$3\exp(-V/20)$ ms^{-1}
γ	150 ms^{-1}
δ	40 ms^{-1}
ε	1.75 ms^{-1}
ζ	$0.03\exp(-V/25)$ ms^{-1}
C_{on}	0.005 ms^{-1}
C_{off}	0.5 ms^{-1}
O_{on}	0.75 ms^{-1}
O_{off}	0.005 ms^{-1}
a	$(O_{on}/C_{on})^{1/4}$
b	$(O_{off}/C_{off})^{1/4}$
Q_{10}	3
T_0	$22°C$
I_{KLVA}, Hodgkin–Huxley model	
w_∞	$1/(1 + \exp(-(V + 67)/8))$
z_∞	$1/(1 + \exp(-(V + 71)/10))$
τ_w	$(100/(6 \times \exp((V + 60)/6) + 16 \times$ $\exp(-(V + 60)/45)) + 1.5$
τ_z	$(100/(\exp((V + 60)/20) + \exp(-(V + 60)/8)) + 50$
Q_{10}	3
T_0	$22°C$
I_{KHVA}, Hodgkin–Huxley model	
n_∞	$1/(1 + \exp(-(V + 42.5)/4.5))$
p_∞	$1/(1 + \exp(-(V + 11.2)/6))$
τ_n	$(100/(11 \times \exp((V + 60)/24) + 21 \times$ $\exp(-(V + 60)/23)) + 0.7$
τ_p	$(100/(4 \times \exp((V + 60)/32) + 5 \times$ $\exp(-(V + 60)/22)) + 5$
Q_{10}	3
T_0	$22°C$

V, C and O denote voltage, closed and opened states, respectively.

0.01433 ms^{-1} to restore I_{NaT} and I_{NaP}, respectively (see Fig. 6*B* and *C*).

Immunocytochemistry

Chicken embryo brains (E11, E15 and E21; $n = 3$ for each age) were dissected out of the skull and immediately immersed in modified periodate–lysin–paraformaldehyde (PLP) fixative: 0.2% (w/v) paraformaldehyde, 2.7% (w/v) lysin HCl, 0.21% (w/v) NaIO$_4$, and 0.1% (w/v) Na$_2$HPO$_4$ (Kuba *et al.* 2005). Brains of all ages were then transferred to 30% sucrose in 0.1 M phosphate buffer for 3 days and sectioned in the coronal plane at 30 μm on a freezing sliding microtome. Each section was collected in 0.01 M phosphate-buffered saline (PBS) with 0.02% sodium azide. Alternate serial sections were immunocytochemically stained for anti-Na$_V$1.6, generously provided by Dr Hiroshi Kuba at Kyoto University (Kuba *et al.* 2006). Briefly, free-floating sections were incubated with primary antibody solutions (1:1000) diluted in PBS with 0.3% Triton X-100 overnight at 4°C, followed by Alexa-Fluor secondary antibodies (Thermo Fisher Scientific, Waltham, MA, USA) at 1:400 overnight at 4°C. Sections from E21 chickens were double stained with Neurofilament 200 (Sigma-Aldrich, N0142). Sections of all ages were then mounted on gelatin-coated slides and coverslipped with Fluoromount-G mounting medium® (Southern Biotech, Birmingham, AL, USA). Images were captured with an Olympus FV1200 confocal microscope. Image brightness, gamma and contrast adjustments were performed in Adobe Photoshop (Adobe Systems, San Jose, CA, USA).

Results

Frequency–firing pattern of NM neurons

Auditory brainstem neurons are able to fire APs at high rates (Oertel, 1997; Trussell, 1997, 1999). Therefore, we first tested whether late-developing NM neurons (E19–21) follow varying frequency rates with high fidelity. Square pulse current trains at frequencies from 50 to 300 Hz were injected into the soma of NM neurons. Firing probability at each frequency was defined as the average number of APs per square pulse (see Methods). The majority of NM neurons (11 out of 12 neurons) were able to follow square pulse trains of 150 Hz in a one-to-one manner (i.e. high-fidelity, Fig. 2*Aa* and *D*). Firing probability dropped to ∼0.6 at 200 Hz when obvious failures of spike generation are observed during the stimulus (Fig. 2*Ca* and *D*, asterisks). When increasing the stimulus frequency
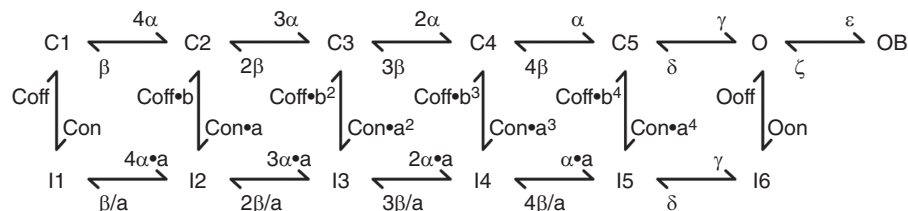

Figure 1. Markovian state model of the sodium (Na$_V$) channel
Reproduced from the model described by Khaliq *et al.* (2003). C, I, O, and OB denote closed, inactivated, open and open-blocked states, respectively. The values of the kinetic parameters are shown in Table 2.

beyond 200 Hz, firing probability was further reduced below 0.5 and in response to 300 Hz stimulation, NM neurons only fired a single onset AP (data not shown). Therefore, NM neurons are capable of firing APs at rates up to 200 Hz with good fidelity, and this ability of frequency firing is similar to other auditory brainstem neurons (Gao & Lu, 2008).

Our current-clamp recordings were conducted at room temperature (~24°C). Chickens have a body temperature of ~42°C. Increasing recording temperature changes the physiology of neurons dramatically (Kushmerick *et al.* 2006). Our previous study recorded APs at near-physiological temperature (~35°C) and we showed a significant improvement of AP kinetics for NM neurons (Hong *et al.* 2016). For example, AP half-width was reduced by ~30% and fall rate increased by ~40% when increasing the temperature to ~35°C. Based on these observations, one would expect that NM neurons recorded at higher temperatures could follow stimulations higher than 200 Hz. Indeed, a recent study using current-clamp

recordings at 38–40°C reveals that NM neurons are able to follow square pulse trains up to 500 Hz with good fidelity, whereas the firing probability drops dramatically at 667 Hz (Kuba *et al.* 2015).

K_V3-containing channels, which belong to the family of K_{HVA} channels, promote the AP repolarizing phase and have been shown to shape the frequency–firing pattern of many neurons (Wang & Kaczmarek, 1998; Johnston *et al.* 2010; Hong *et al.* 2016). Based on previous findings, we hypothesized that K_V3-containing channels play a major role in regulating the rapid firing capability NM neurons. To test this hypothesis, we bath applied TEA (1 mM) to block K_V3-containing channels. Representative responses to 150 Hz square pulse trains before and during TEA application are shown in Fig. 2*Aa* and *b*. The enlargement of two overlaid APs from the same neuron is shown in Fig. 2*B*. During TEA application, the majority of NM neurons (10 out of 12 neurons) were still able to follow pulse trains of 150 Hz with 100% fidelity, despite a significant widening of APs ($P = 0.0034$, Fig. 2*B* and *D*).
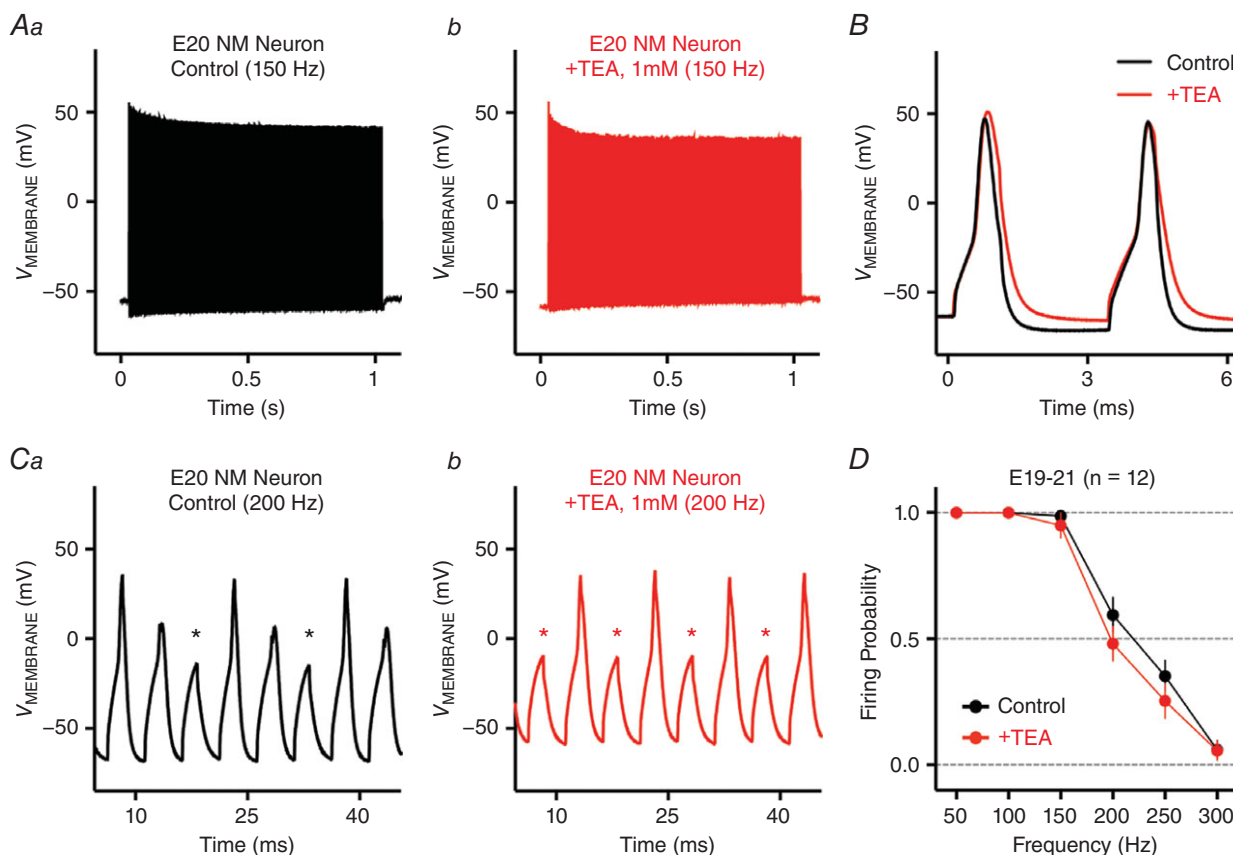
**Figure 2. Frequency–firing pattern of NM neurons at E19–21**
Aa and *b*, representative voltage responses recorded from an E20 NM neuron to current injections of square pulse trains at 150 Hz, before and during TEA (1 mM) application, respectively. *B*, overlaid enlargement of representative voltage responses shown in *Aa* and *b*. *Ca* and *b*, representative voltage responses to current injections of square pulse trains at 200 Hz, before and during TEA application, respectively. Asterisk indicates action potential failure. *D*, population data showing firing probability of NM neurons as a function of square pulse frequency. The strength of all square pulse trains is 1 nA with a duration of 1 s. Individual square pulse width is 2 ms. Error bar, SEM.

Correspondingly, no changes in firing probability at 50 or 100 Hz were observed with blockade of K_V3-containing channels (Fig. 2D). In contrast, we observed reduction in firing probability when increasing the stimulus frequency to 200 or 250 Hz (Fig. 2Ca and b and D). In response to 200 Hz stimulation, firing probability was reduced by ∼19% on average. Although this reduction is statistically significant ($P = 0.0011$), nearly half of the recorded neurons (5 out of 12 neurons) showed a reduction of only ∼10% or less in firing probability. These observations with TEA application indicate that K_V3-containing channels contribute partially to higher frequency firing of NM neurons and thus gave rise to an important question: what

other factor(s) regulate the ability of NM neurons to follow inputs up to 200 Hz with relatively high fidelity?

Resurgent Na_V current of NM neurons

A number of previous studies suggest that I_{NaR} shapes the rapid firing and burst generation in many mammalian neurons (Lewis & Raman, 2014). Therefore, we speculated that NM neurons have I_{NaR}, which is likely one of the factors that regulate the frequency–firing pattern of NM neurons. We first examined whether I_{NaR} is present in NM by using classic voltage-clamp protocols (Raman & Bean, 1997; Fig. 3). NM neurons were held at
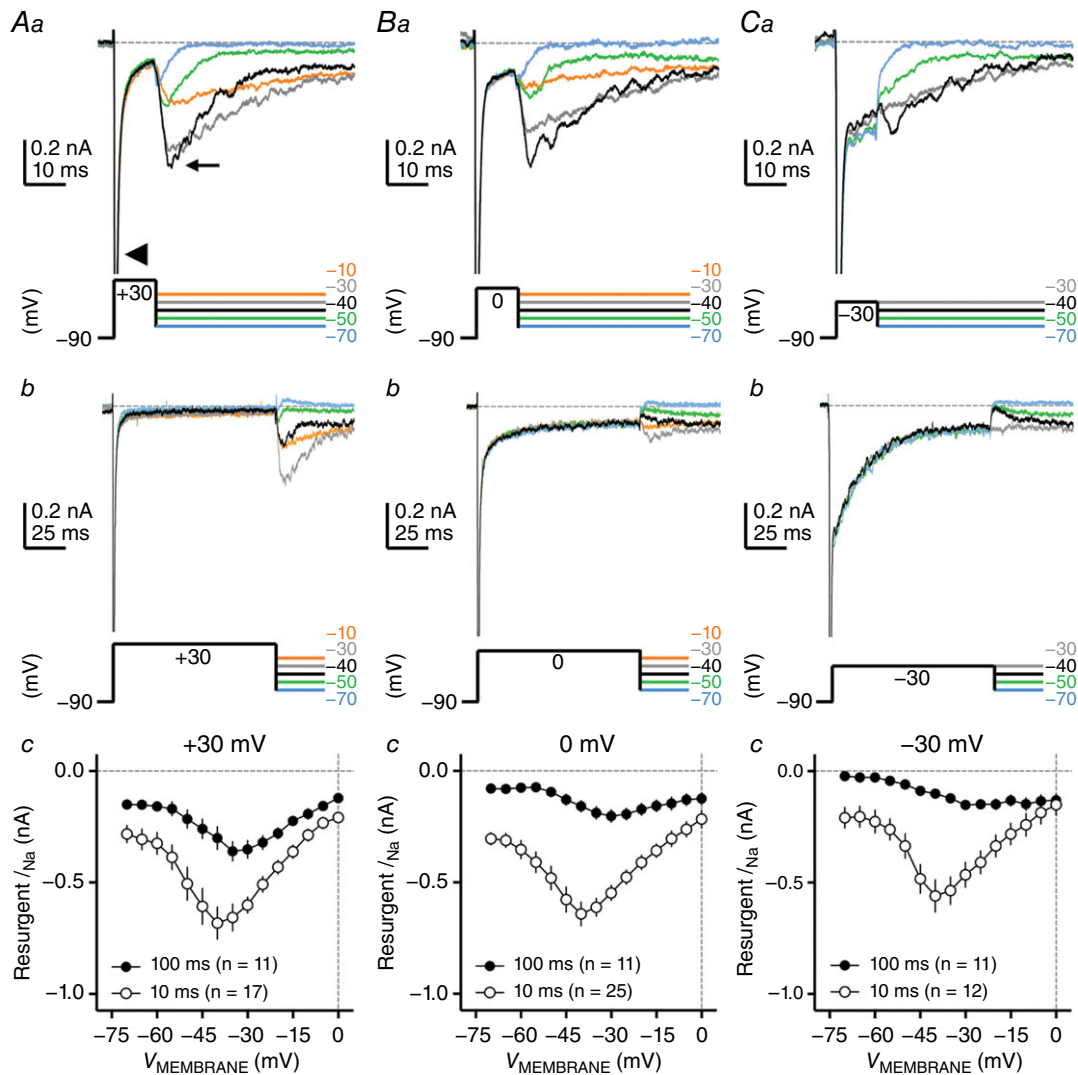
Figure 3. Resurgent sodium current (I_{NaR}) of NM neurons at E19–21
Aa and *b*, *Ba* and *b* and *Ca* and *b*, representative current traces in response to voltage-clamp protocols that elicit I_{NaR} shown below traces. The amplitude of the conditioning step is +30 mV in *Aa* and *b*, 0 mV in *Ba* and *b* and −30 mV in *Ca* and *b*. The duration of the conditioning step is 10 ms in *Aa–Ca* and 100 ms in *Ab–Cb*. Arrowhead and small arrow in *Aa* indicate the transient sodium current (I_{NaT}) and I_{NaR}, respectively. *Ac*, *Bc* and *Cc*, population data showing the I_{NaR} amplitude as a function of repolarizing membrane voltage ($V_{MEMBRANE}$) in response to the conditioning steps shown in *Aa* and *b*, *Ba* and *b* and *Ca* and *b*, respectively. Error bar, SEM.

−90 mV before giving a depolarizing conditioning step to +30 mV (duration = 10 ms). A transient Na$_V$ current (I_{NaT}) was evoked by the conditioning step (Fig. 3*Aa*, arrowhead). Afterwards, neurons were repolarized to varying membrane voltages from −70 mV to 0 mV (Δ step = 5 mV). Inward-going I_{NaR}, which could be eliminated by TTX application, was elicited by repolarization and its amplitude was plotted as a function of repolarizing membrane voltage (Fig. 3*Aa*, small arrow, and *Ac*). The I–V curve of I_{NaR} for NM neurons peaked at −40 mV and presented with the typical 'V' shape that largely resembled that of I_{NaR} reported in mammalian neurons (Lewis & Raman, 2014). The maximal amplitude of I_{NaR} is usually less than 1 nA for NM neurons recorded from slice preparation, which is much smaller than the amplitude of I_{NaT} (Fig. 3*Ac*). This property is also similar to that observed in other auditory brainstem neurons (Leao *et al.* 2006; Kim *et al.* 2010). Therefore, by using the conditioning step of +30 mV at 10 ms, NM neurons show robust generation of I_{NaR} that is present with similar amplitude and voltage dependence properties to mammalian neurons.

In mammalian neurons, the I_{NaR} amplitude is dependent on the duration and level of the conditioning step (Raman & Bean, 2001). This is due to two competing inactivation mechanisms of Na$_V$ channels: open channel block induced by an intracellular particle and the classic inactivation induced by the 'gate' (i.e. cytoplasmic III–IV linker) within the α-subunit. As demonstrated in cerebellar Purkinje cells, the majority of Na$_V$ channels will be open channel blocked if neurons are exposed to a short and more positive depolarization (e.g. an AP). The unbinding of open channel block at moderately negative membrane voltage (e.g. −40 mV) under this condition generates large I_{NaR}. With longer and less positive depolarization, Na$_V$ channels will mainly adopt the classic inactivation gate that requires hyperpolarization of membrane voltage to be released, and the generation of I_{NaR} will be minimal. In order to investigate whether I_{NaR} in NM has similar properties, we applied conditioning steps with different durations and levels and compared

the I_{NaR} amplitude among the conditions. For example, the duration of +30 mV depolarization was extended from 10 to 100 ms. Fig. 3*Ab* shows representative current traces in response to the prolonged conditioning step. The generation of I_{NaR} can still be observed but with a smaller amplitude. Indeed, comparison between the two I–V curves revealed a significant reduction in current amplitude when the conditioning step was elongated to 100 ms (Fig. 3*Ac*). Interestingly, we also observed a shift in peak membrane voltage towards the positive direction by ∼5 mV.

Next, we changed the level of the conditioning step to 0 mV and −30 mV while maintaining the same duration (i.e. 10 ms). Fig. 3*Ba* and *Ca* shows representative current traces in response to conditioning steps of 0 mV and −30 mV, respectively. By comparing the I–V curves shown in Fig. 3*Ac–Cc*, we observed a decreasing trend (albeit not significant) in I_{NaR} amplitude when the conditioning step was switched from positive to negative voltages. The voltage dependence did not change with different levels of conditioning steps (i.e. all peaked at −40 mV). Finally, we applied a long duration (i.e. 100 ms) conditioning step at non-positive levels (i.e. 0 and −30 mV), with the prediction that Na$_V$ channels will be unlikely to adopt the open channel block and thus elicit minimal I_{NaR}. Indeed, a dramatic reduction in current amplitude was observed in both cases (Fig. 3*Bb* and *c* and *Cb* and *c*) along with a shift in voltage dependence by ∼10 mV. Under the condition of −30 mV, the reduction was so great that the typical 'V' shape of the I_{NaR} I–V curve was lost (Fig. 3*Cc*), which can be explained by the following two factors. First, I_{NaR}, if any, was hardly detectable in response to the conditioning step of −30 mV at 100 ms (Fig. 3*Cb*). Instead, steady-state current was evident following the repolarization. Second, low-level contaminant noise and/or other channel conductances can obscure small I_{NaR}, which prevents the amplitude of I_{NaR} from being reliably measured (Afshari *et al.* 2004; Aman *et al.* 2009).

We further characterized the kinetics of I_{NaR}, which is considered to be another important property. Two
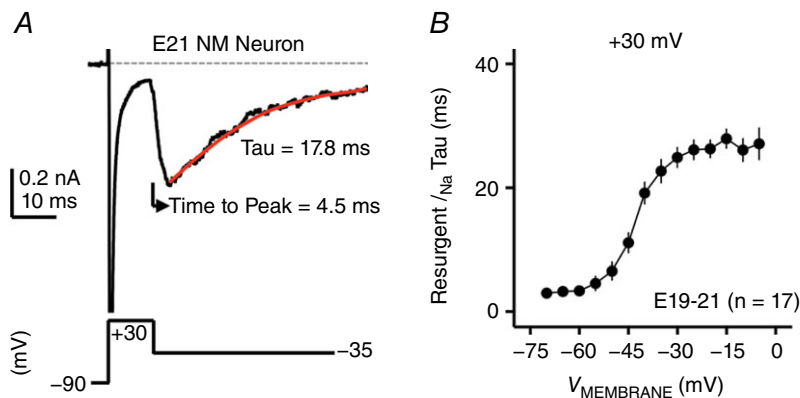
Figure 4. I_{NaR} kinetics of NM neurons at E19–21
A, representative current trace showing the calculation of time to peak and decay time constant (tau) for I_{NaR}. Decay time constant (tau) is obtained by fitting a single exponential (red trace) to the decay phase of I_{NaR}. The conditioning step is +30 mV at 10 ms. B, population data showing the decay time constant (tau) of I_{NaR} as a function of repolarizing membrane voltage ($V_{MEMBRANE}$). Error bar, SEM.

variables of kinetics were used based on previous studies: time to peak and decay time constant (tau; Raman & Bean, 1997; Lewis & Raman, 2011). Fig. 4*A* shows the calculation of two variables in the current study. Time to peak is defined as the time interval between the onset of repolarization and the I_{NaR} peak. Decay time constant was calculated by fitting a single exponential to the decay phase of I_{NaR}. All calculations were conducted under the conditioning step of +30 mV at 10 ms. Across the population of NM neurons, the average time to peak was 3.97 ± 1.19 ms when measured at the membrane voltage that elicited the maximum current. The membrane voltage for the representative trace shown in Fig. 4*A* was −35 mV. The decay time constant was plotted as a function of repolarizing membrane voltage (Fig. 4*B*). Again, similar to mammalian neurons, the decay time constant of I_{NaR} increased with more depolarized membrane voltage and was generally larger than the decay variable of I_{NaT} (Ming & Wang, 2003; Rush *et al.* 2005), which confirmed the slower kinetics of I_{NaR}. In summary, these observations suggest that the use of the open channel blocker, the inactivation mechanisms and the I_{NaR} kinetics of NM neurons closely resemble those of mammalian neurons, properties likely conserved across various species and neural structures.

Function of resurgent Na_V current for NM neurons: experimental results

We hypothesized that I_{NaR}, along with the underlying open channel blocker, plays an important role in promoting the AP firing rates of NM neurons. We predicted that a neuron's activation of open channel blocker would promote Na_V channel availability and recovery from depolarization, which is ultimately important for subsequent and rapid AP firing. Therefore, we applied two voltage-clamp protocols based on previous studies to test our prediction (Raman & Bean, 2001; Patel *et al.* 2015). In the first protocol, NM neurons were held at −90 mV before being depolarized to +30 mV for 5 ms (Fig. 5). According to our previous observations (see Fig. 3), this conditioned the majority of Na_V channels to be occupied by the open channel blocker (referred here as the 'open channel block state'). The membrane voltage was then set at −65 mV for NM neurons to recover. The recovery time varied from 2 to 50 ms (Δ step = 2 ms). Finally, a depolarization to 0 mV was applied to evoke an I_{NaT}. In the second protocol, the conditioning step was changed to −30 mV for 40 ms, in order to maximize the occupancy of the classic inactivation gate (referred to here as the 'inactivation state'). Fig. 5*A* and *B* shows representative current traces in response to the two protocols from the same neuron. When neurons were given a short and positive conditioning step, abrupt repolarization to the resting state resulted in an obvious generation of I_{NaR} (arrow in Fig. 5*A*), while this was not observed when conditioned to the inactivation

state (Fig. 5*B*). The generation of I_{NaR} further supported the expectation that the occupancy of the open channel blocker was primary for the first protocol.

To determine Na_V channel availability under the two protocols, we calculated the normalized ratio, which indicates the amount of available Na_V channels after the recovery period. To do this, a reference pulse to 0 mV was applied to NM neurons prior to the implementation of the two protocols described above, and the amplitude of I_{NaT} after the recovery was normalized to this 'reference amplitude'. The normalized ratio was plotted as a function of the recovery time in Fig. 5*C*. We observed a clear separation of recovery trajectories between the two conditions, which indicates that the presence of open channel block significantly increased Na_V channel availability during the recovery. The recovery trajectory was fit with a single exponential in order to obtain a recovery time constant (tau). The open channel block significantly shortened the recovery time constant, facilitating the recovery of Na_V channels (Fig. 5*D*). These observations provide supporting evidence for our prediction that the use of the open channel blocker can promote the availability and recovery of Na_V channels.

In addition, we found that the distinction between the two states was larger when the amount of recovery time was short. For example, when NM neurons were only given 2 ms to recover, the availability of Na_V channels was reduced by ∼67% on average from the open channel block state to the inactivation state (Fig. 5*E*, left). But this difference reduced to ∼20% when the recovery time was longer than 20 ms (Fig. 5*E*, middle and right). This suggests that the role of open channel block in recovering Na_V channels is more critical when the recovery time is limited, which is reminiscent of a highly restricted interspike interval when NM neurons are performing rapid auditory tasks (Warchol & Dallos, 1990; Jones & Jones, 2000).

Function of resurgent Na_V current for NM neurons: computational results

We further used a computational model to examine the function of I_{NaR} in NM. This model is designed based on our previous study (Lu *et al.* 2017), in combination with the I_{NaR} model from Khaliq *et al.* (2003). The model NM neuron was held at −90 mV before giving a depolarizing conditioning step to +30 mV (duration = 10 ms). An I_{NaT} was evoked by the conditioning step (Fig. 6*Aa*, arrowhead). The model NM neuron was then repolarized to varying membrane voltages from −70 mV to 0 mV (Δ step = 5 mV). The model NM neuron displayed slightly smaller I_{NaR} amplitudes (Fig. 6*Aa*, small arrow) but comparable voltage dependence properties to our experimental data (Figs 6*Ab* and 3*Ac*). In order to remove I_{NaR}, we first set the rate constant ε to zero (see Fig. 1
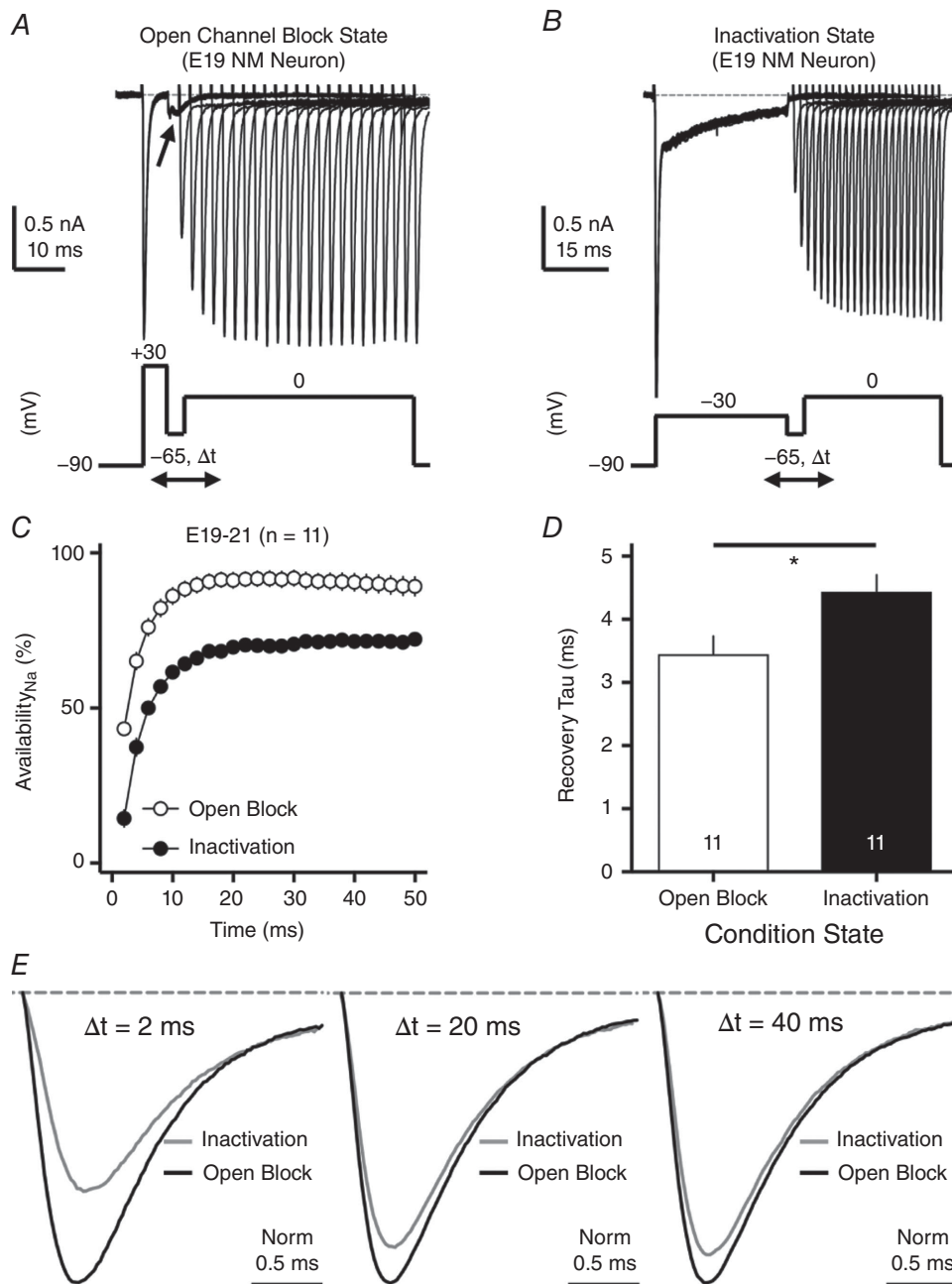
Figure 5. I_{NaR} helps increase Na_V channel availability and facilitates Na_V recovery
A and *B*, representative current traces in response to voltage-clamp protocols shown below traces. The conditioning step is +30 mV at 5 ms in *A* (open channel block state) and −30 mV at 40 ms in *B* (inactivation state). Δ*t* represents the varying recovery time, increasing from 2 to 50 ms in steps of 2 ms. Arrow in *A* indicates the generation of I_{NaR}. *C*, population data showing the Na_V channel availability (%) as a function of recovery time. In order to calculate Na_V channel availability, a reference pulse to 0 mV was applied to NM neurons (not shown in the figure), and the amplitude of I_{NaT} after the recovery was normalized to this 'reference amplitude'. Before the normalization, the amplitude of I_{NaT} was first adjusted by subtracting the steady-state current that remained at the end of the conditioning step. The recovery trajectory is fit by a single exponential, in order to obtain recovery time constant (tau) shown in *D*. *D*, population data showing the recovery time constant (tau) under two different condition states. *P < 0.05. Numbers on bars represent sample size. *E*, representative current traces shown in *A* and *B* are normalized and overlaid for recovery time periods of 2 ms (left), 20 ms (middle) and 40 ms (right). Error bar, SEM.

for reference). This modification, however, significantly slowed down the falling phase of I_{NaT} (Fig. 6B, the '0-I_{NaR-}' condition, blue trace). The slower falling phase of I_{NaT} is because the Markovian 13-state Na$_V$-channel model sets the O→OB transition (with the rate constant ε, see Fig. 1) as a major exit path from the open state (Magistretti *et al.* 2006). Removing this path resulted in the slower speed of channels exiting the open state and thus led to a slower I_{NaT} falling phase. Therefore, we next increased the rate constant O_{on} to 2.15 ms^{-1} and the O_{off} to 0.01433 ms^{-1} to restore the normal decay kinetics of I_{NaT} and amplitude of I_{NaP}, respectively (Fig. 6B and C, the '0-I_{NaR+}' condition, red trace). After these two modifications, I_{NaR} was successfully eliminated (Fig. 6C). Both 0-I_{NaR-} (blue) and 0-I_{NaR+} (red) conditions were used to characterize the spiking activity of model NM neuron without I_{NaR}. The only difference between 0-I_{NaR+} and control conditions was the absence of I_{NaR}, while the 0-I_{NaR-} condition showed both the absence of I_{NaR} and slower I_{NaT} decay kinetics.

Our model NM neuron generated similar voltage responses to square pulse current trains with varying frequencies, as compared to our experimental data. For example, the model NM neuron responded to a 200 Hz current injection with ~0.6 AP firing probability (Fig. 7Aa and c). It should be noted that an AP was identified only if the evoked voltage peak exceeded −30 mV. Voltages below this value were considered as failures (Fig. 7Ac, asterisks). Fig. 7Ab shows the total underlying Na$_V$ current required for AP generation in Fig. 7Aa. With the current and time scale expanded, we observed a clear but small inward Na$_V$ current immediately after a large I_{NaT} (Fig. 7Ad, arrow). This inward Na$_V$ current is reminiscent of I_{NaR} that occurs during the AP repolarizing phase and closely resembles the data reported by previous 'AP-clamp' studies in mammalian neurons (Raman & Bean, 1997, 1999). When we removed I_{NaR} in the model NM neuron, the reduction in firing probability was identical in both 0-I_{NaR-} and 0-I_{NaR+} conditions. Firing probability at 200 Hz was reduced by ~21% (Fig. 7Ba–c, asterisks; Fig. 7Ca–c, asterisks) and the small inward Na$_V$ current after I_{NaT} was no longer visible (Fig. 7Bd and Cd, arrow). This result further confirmed that the small inward current is I_{NaR} and is induced by the mechanism of open channel block. In addition, when we removed both I_{NaR} and K$_{HVA}$ currents, firing probability in response to 200 Hz stimulation was reduced by ~23% from the control – just slightly larger than the reduction we observed with I_{NaR} removal only (data not shown).

It should be noted that I_{NaT} generated in the 0-I_{NaR-} condition was obviously wider than in the 0-I_{NaR+} condition, though the same amount of reduction in firing

Figure 6. Simulations of Na$_V$ currents from the model NM neuron
Aa, simulated current traces (upper panel) in response to the voltage-clamp protocol (lower panel) consisting of a 10 ms conditioning step to +30 mV, followed by step repolarizations to −10, −30, −40, −50 and −70 mV. Arrowhead and small arrow indicate I_{NaT} and I_{NaR}, respectively. *Ab*, current–voltage relationship of simulated I_{NaR}. *B*, simulated I_{NaT} (upper panel) was evoked by depolarizing steps to 0 mV (lower panel). The current obtained under control condition is shown in black. Switching off I_{NaR} by setting the rate constant for the O→OB transition, ε, to 0 resulted in considerable slowing of I_{NaT} decay (0-I_{NaR-} condition, blue trace). I_{NaT} was restored under 0-I_{NaR+} condition ($\varepsilon = 0$, $O_{on} = 2.15$ ms^{-1}, and $O_{off} = 0.01433$ ms^{-1}; red trace). *C*, simulated I_{NaR} under control (black trace) and 0-I_{NaR+} condition (red trace). Removal of I_{NaR} under the 0-I_{NaR+} condition has no effect on persistent Na$_V$ current (I_{NaP}).
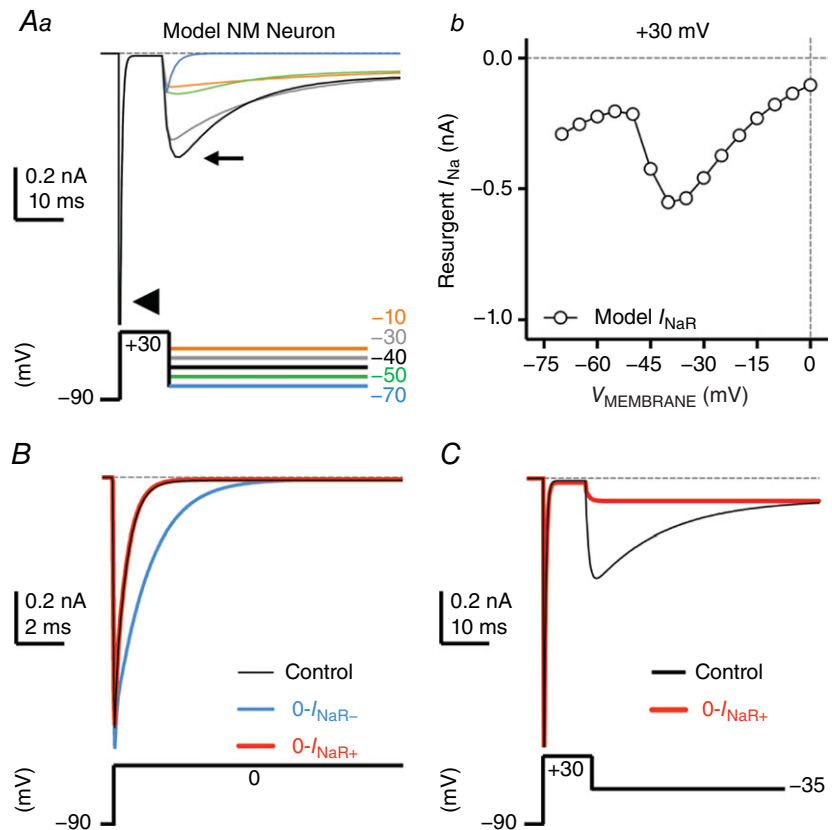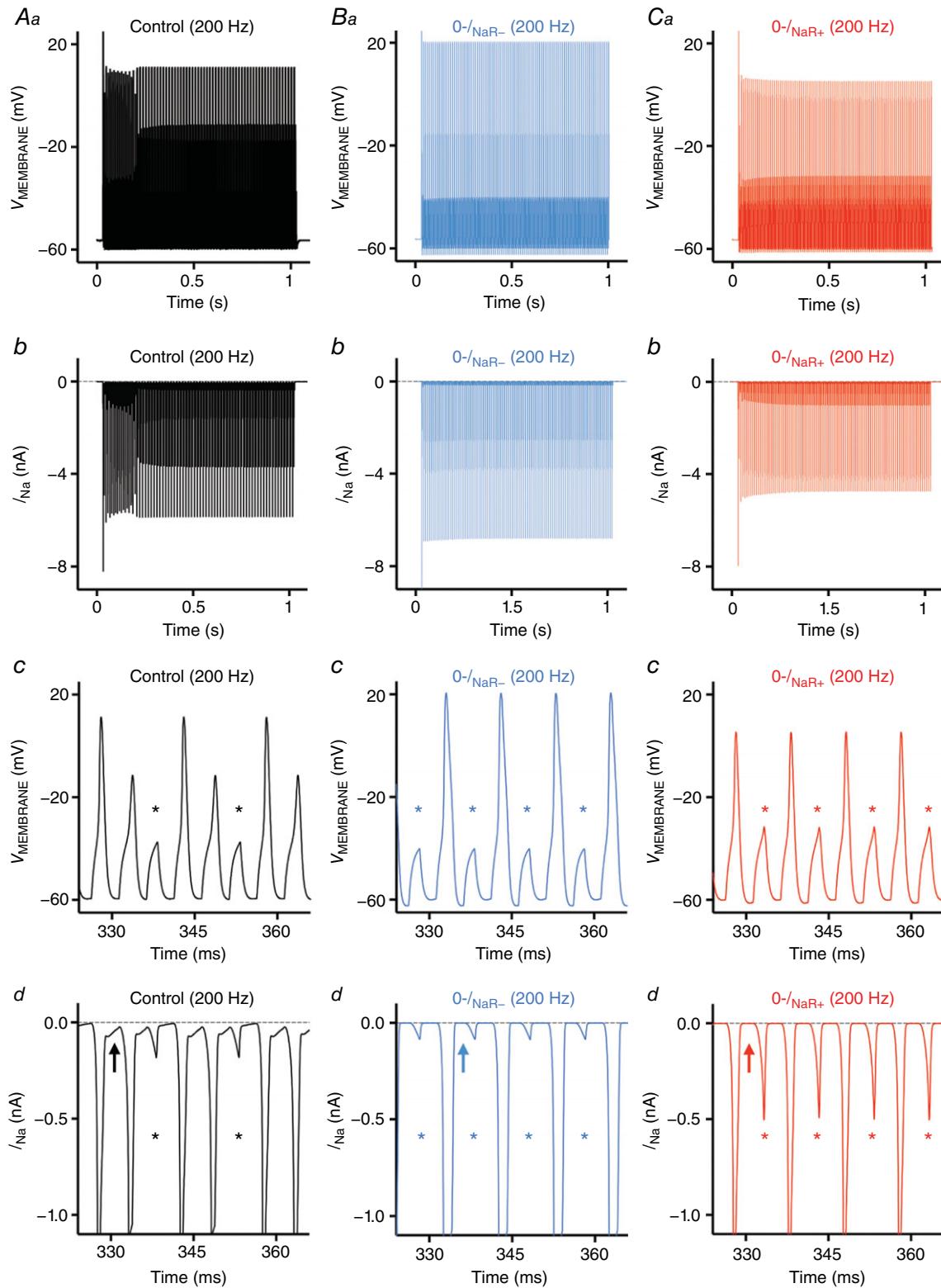
Figure 7. I_{NaR} promotes frequency firing of model NM neuron

Aa–d, *Ba–d* and *Ca–d*, simulated voltage and current responses to square pulse current injections of 200 Hz, under the control, 0-I_{NaR-} (i.e. I_{NaR} removal and slower I_{NaT}) and 0-I_{NaR+} (i.e. I_{NaR} removal) conditions, respectively. *Aa*, *Ba* and *Ca* are model output of membrane voltage ($V_{MEMBRANE}$); enlarged traces shown in *Ac*, *Bc* and *Cc*. *Ab*, *Bb* and *Cb* are model output of Na$_V$ currents; enlarged traces are shown in *Ad*, *Bd* and *Cd*. Asterisk indicates action potential failure. Arrows indicate the generation (*Ad*) or elimination (*Bd* and *Cd*) of I_{NaR}.

probability was observed for both conditions (Fig. 7*Bd* and *Cd*). This difference is due to the slower decay kinetics of I_{NaT} in the 0-I_{NaR-} condition that means Na$_V$ channels inactivate more slowly (see Fig. 6*B*). As a result, APs generated in the 0-I_{NaR-} condition showed longer half-width and larger amplitude than in the 0-I_{NaR+} condition (Fig. 7*Bc* and *Cc*). In addition, we also observed a difference between two conditions in a small I_{NaT} that failed to generate an AP after a large I_{NaT} (Fig. 7*Bd* and *Cd*, asterisks). In the 0-I_{NaR-} condition, Na$_V$ currents after a large I_{NaT}, the amplitude of which indicates the number of Na$_V$ channels recovered after an AP, were present with smaller amplitude than those in the 0-I_{NaR+} condition (Fig. 7*Bd* and *Cd*, asterisks). This is because of the slower Na$_V$ channel kinetics in the 0-I_{NaR-} condition and the highly restricted recovery time in response to 200 Hz square pulse trains. Nevertheless, the identical reduction in firing probability in both conditions confirmed that the reduced ability of the model NM neuron to follow inputs at high rates was not due to a slower I_{NaT} but to the absence of I_{NaR}. Together, our modelling results indicate that I_{NaR} helps shape AP firing rate of NM neurons.

Development of resurgent Na$_V$ current in NM

We confirmed the generation of I_{NaR} in late-developing NM neurons (i.e. E19–21), when near-mature hearing ability is established (Jones *et al*. 2006). Next, we investigated whether NM neurons in the earlier periods of development have I_{NaR}. Voltage-clamp experiments were first performed on NM neurons at E14–16, which corresponds to a developmental period when crude hearing ability is just established for chickens (i.e. during hearing onset). To our surprise, we observed robust generation of I_{NaR} at E14–16 when using the conditioning step of +30 mV, 10 ms, with the peak amplitude just slightly smaller than that of late-developing NM neurons (Fig. 8*A* and *D*). Also similar to late-developing neurons, the I_{NaR} amplitude was reduced when we changed the level of the conditioning step to either less positive voltages (i.e. 0 and −30 mV) or extended the step duration (i.e. 10 and 100 ms) (Fig. 8*A* and *B* and *D*–*F*). Additionally, we observed a shift in the peak of *I*–*V* curve in the positive direction by ∼15 mV when we prolonged the duration of the step from 10 to 100 ms. These observations
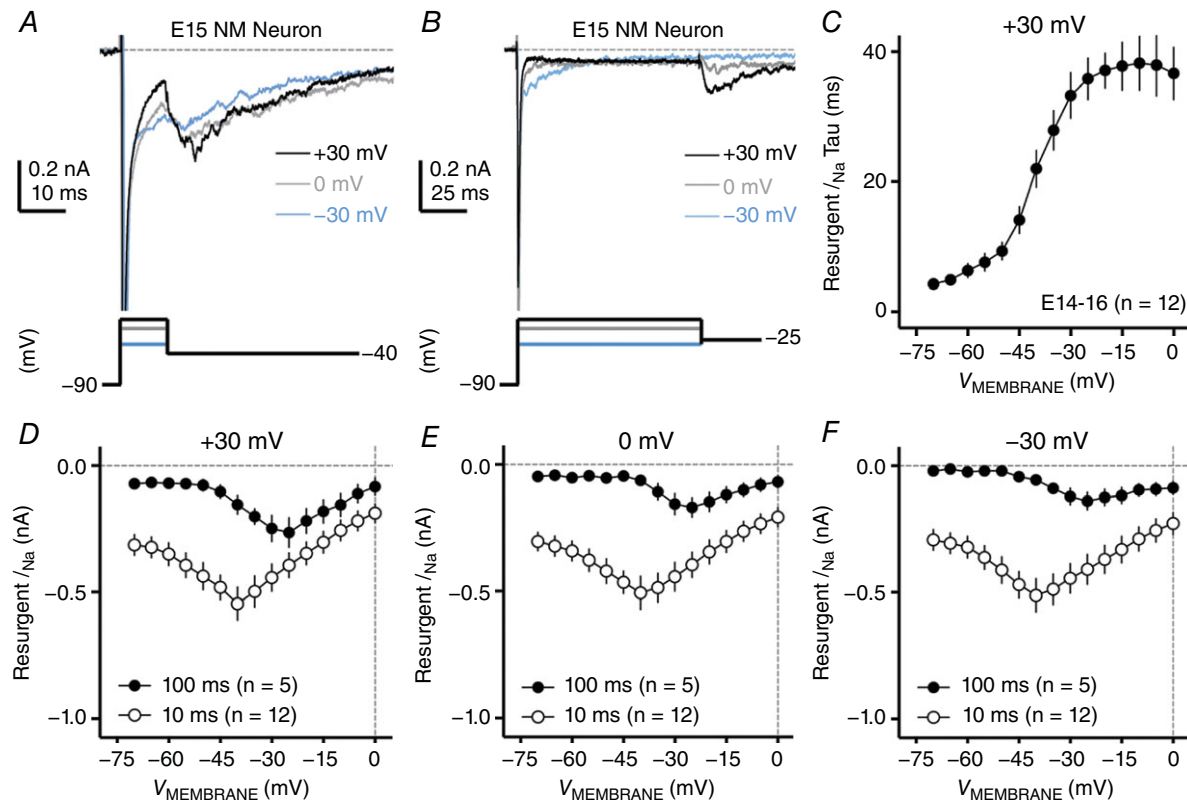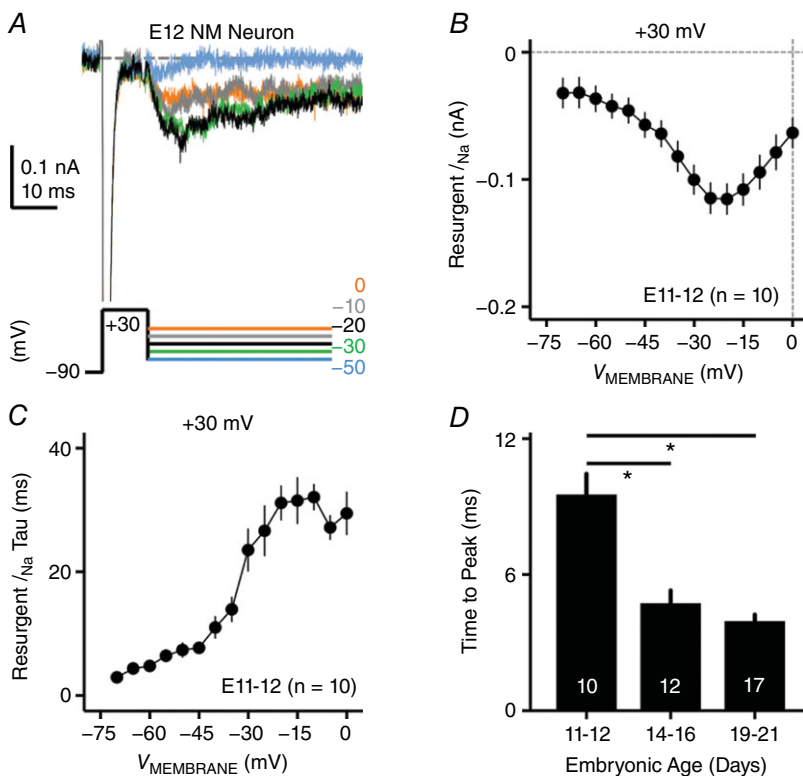

Figure 8. I_{NaR} properties of NM neurons at E14–16
A and *B*, representative current traces in response to voltage-clamp protocols shown below traces. The strength of the conditioning step is +30 mV (black trace), 0 mV (grey trace) and −30 mV (blue trace) and the duration is 10 ms in *A* and 100 ms in *B*. *C*, population data showing the decay time constant (tau) of I_{NaR} as a function of repolarizing membrane voltage ($V_{MEMBRANE}$). *D*–*F*, population data showing the I_{NaR} amplitude as a function of repolarizing membrane voltage ($V_{MEMBRANE}$) in response to different conditioning steps. The strength of the conditioning step is +30 mV in *D*, 0 mV in *E* and −30 mV in *F*, and the duration is 10 and 100 ms. Error bar, SEM.

suggest that during hearing onset, the mechanisms of open channel block are established and show near-mature properties.

Despite these similarities, we also noticed that some properties of I_{NaR} at E14–16 were different from late-developing neurons. It should be noted that the following differences are discussed using the conditioning step of +30 mV, 10 ms. Although the I_{NaR} amplitude peaked at −40 mV for both age groups, it reduced more dramatically at older ages when membrane voltage became more positive or more negative (see Figs 3*Ac* and 8*D*). According to a previous study (Lewis & Raman, 2011), the relative amplitude of I_{NaR} depends on two mechanisms. First, the rate of the open channel block unbinding from the Na_V channel α-subunit, which indicates the affinity between these two particles, and second, after removal, the rate of the α-subunit entering the classic inactivation or closed states (depending on the voltage). Time to peak is a good index for the first mechanism (i.e. the rate of unbinding), while decay time constant is dependent on both mechanisms. We did not observe a significant difference of time to peak between two age groups (see Fig. 9*D*, $P = 0.88$). Furthermore, we plotted the decay time constant as a function of membrane voltage for E14–16 NM neurons and compared it with E19–21 NM neurons (Figs 8*C* and 4*B*, respectively). Indeed, E14–16 NM neurons showed a generally larger decay time constant than the older age group. Therefore, we suggest that Na_V channels at E14–16 inactivate or close (at the membrane voltage more positive or more negative than −40 mV, respectively) significantly slower after the unbinding of the open channel blocker, resulting in a less dramatic fall-off of I_{NaR} amplitude and thus a shallower slope of their *I–V* curve than Na_V channels at E19–21. Although additional experiments are required to test this suggestion, we speculate that longer I_{NaR} decay kinetics are partially related to the type of Na_V α-subunit(s) expressed at E14–16 compared to older ages (see below).

Next, we performed voltage-clamp experiments on NM neurons at E11–12, when chickens are not able to respond to sound (i.e. before hearing onset; Jones *et al.* 2006). In 10 out of 14 recorded neurons, we observed small I_{NaR} when using the conditioning step of +30 mV, 10 ms (Fig. 9*A*, note scale). The maximal amplitude of I_{NaR} was slightly above 100 pA, which is dramatically smaller than the current amplitude of the other two age groups (Fig. 9*B*). In addition, the voltage dependence of I_{NaR} at E11–12 was very different from the other two age groups, showing an obvious shift in peak voltage (i.e. at −20 mV, Fig. 9*B*). Fig. 9*C* shows the decay time constant of I_{NaR} for NM neurons before hearing onset, which presented with an increasing trend with more depolarized membrane voltage. Time to peak was 9.54 ± 2.87 ms when measured at the maximal I_{NaR}. This value is significantly larger than those of the other two age groups, indicating a stronger affinity between the open channel blocker and the α-subunit of Na_V channels, and thus slower kinetics of I_{NaR}

Figure 9. I_{NaR} properties of NM neurons at E11–12

A, representative current traces in response to voltage-clamp protocols shown below traces. The conditioning step is +30 mV at 10 ms. *B*, population data showing the current amplitude as a function of repolarizing membrane voltage ($V_{MEMBRANE}$) in response to conditioning step of +30 mV at 10 ms. *C*, population data showing the decay time constant (tau) of I_{NaR} as a function of repolarizing membrane voltage ($V_{MEMBRANE}$). *D*, population data showing time to peak of I_{NaR} at different embryonic ages. *$P < 0.05$. Numbers on the bars represent sample size. Error bar, SEM.

Table 3. Sodium channel current properties

Amplitude	E11–12 (n)	E14–16 (n)	E19–21 (n)	ANOVA
Transient I_{NaV}[a] (nA)	-1.57 ± 0.13 (7)	-2.65 ± 0.30 (12)	-3.85 ± 0.40 (12)	$P = 0.0005$
Resurgent I_{NaV}[b] (nA)	-0.10 ± 0.01 (10)	-0.44 ± 0.05 (12)	-0.60 ± 0.04 (17)	$P < 0.0001$
Persistent I_{NaV}[b,c] (nA)	-0.05 ± 0.01 (10)	-0.12 ± 0.02 (12)	-0.14 ± 0.01 (16)	$P = 0.001$

[a]Transient Na_V current = amplitude calculated at step depolarization to -30 mV (holding voltage = -90 mV). [b]Resurgent and persistent Na_V current = amplitude calculated at the repolarizing membrane voltage of -30 mV. The conditioning step = $+30$ mV for 10 ms. [c]Persistent Na_V current = measured at the end of the 100 ms repolarizing membrane voltage.

at E11–12 (Fig. 9*D*). Taken together, during the prehearing period, I_{NaR} was present in the majority of NM neurons with preliminary properties. With development, the I_{NaR} amplitude increased, kinetics improved and its voltage dependence shifted towards negative direction. By the time of hearing onset, NM neurons obtained more mature-like I_{NaR} properties. Table 3 summarizes the developmental changes in amplitude of I_{NaT}, I_{NaR} and I_{NaP}, when measured at membrane voltage of -30 mV. The amplitude of I_{NaP} was measured at the end of 100 ms repolarization after the conditioning step ($+30$ mV, 10 ms). We observed significant increases in all three current amplitudes for NM neurons as a function of development.

Development of frequency–firing pattern in NM

Based on the functional role of I_{NaR} and its development in NM, we predicted that neurons at the age of E14–16 would show similar frequency–firing pattern with late-developing neurons (i.e. E19–21), whereas neurons at E11–12 would not be able to follow square pulse frequency as high as the other two age groups, due to their underdeveloped I_{NaR} (see Fig. 9) and K_V channels (Hong *et al.* 2016). To test this prediction, we first applied the aforementioned current commands of square pulse trains to NM neurons at E14–16. As expected, neurons at this age were able to follow square pulse trains of 150 Hz in a one-to-one manner (Fig. 10*Aa* and *c*). Firing probability dropped continuously when stimulus frequency was higher than 150 Hz (Fig. 10*Ac*). In response to square pulse trains of 200 and 250 Hz, firing probabilities were ∼0.5 and ∼0.25, respectively (Fig. 10*Ab* and *Ac*), which are slightly lower than those of E19–21 NM neurons but these differences are not statistically significant ($P = 0.49$ and 0.32, respectively). When the stimulus frequency was 300 Hz, E14–16 NM neurons showed a single onset spike similar to late-developing neurons (data not shown).

For NM neurons at E11–12, individual square pulse width was extended to 5 ms because neurons at this age are present with average AP half-width of ∼4.6 ms (Hong *et al.* 2016). We found that NM neurons at E11–12 were able to follow square pulse trains with good fidelity up to 70 Hz (Fig. 10*Bc*). Fig. 10*Ba* shows a representative

E12 neuron that was able to reliably generate an AP in response to each pulse of the 70 Hz stimulation. When stimulus frequency was increased to 100 Hz or higher, however, firing probability dropped steeply below 0.5 and in response to 150 Hz stimulation, NM neurons at E11–12 only generated a single onset spike followed by membrane oscillations at a depolarized level (Fig. 10*Bb* and *c*). This is in stark contrast to the other two age groups, which could follow 150 Hz square pulse trains in a reliable manner (see Figs 2*D* and 10*Ac*). Taken together, NM neurons at E14–16 showed a frequency–firing pattern closely resembling their late-developing counterparts, while the ability of NM neurons at E11–12 to follow high-frequency stimulations was markedly limited. These results are similar to our previous data, which show that E11–12 NM neurons are most responsive to low-frequency (<40 Hz) sinusoidal current injections (Hong *et al.* 2016).

Expression of Na_V1.6 channels

Na_V1.6 channels are extensively expressed in the mammalian central nervous system and act as a predominant carrier for I_{NaR} (Eijkelkamp *et al.* 2012; Lewis & Raman, 2014). Therefore, we explored whether Na_V1.6 channels are expressed in developing NM, using an antibody specifically recognizing chicken Na_V1.6 (Kuba *et al.* 2006, 2010, 2014). In late-developing NM neurons (i.e. E21), strong Na_V1.6 immunoreactivity was observed as bright punctate segments (Fig. 11*Aa* and *b*). Because E21 NM neurons are mostly adendritic (Jhaveri & Morest, 1982*a*), double staining of Na_V1.6 and neurofilament further demonstrated that Na_V1.6 is localized in neurofilament-stained NM axons that can be traced back to the cell bodies (Fig. 12). These Na_V1.6-containing segments closely resembled the characterized distribution pattern of Na_V1.6 in chicken auditory brainstem as reported by Kuba *et al.* (2010, 2014) and possibly represented the axon initial segments (AIS) and nodes of Ranvier. In contrast, the Na_V1.6-containing segments were absent in NM at E15 (Fig. 11*Ba* and *b*) and E11 (Fig. 11*Ca* and *b*). In addition, NM cell bodies contained a low level of Na_V1.6 immunoreactivity at E21, which became increasingly less distinct from E21 to E15 and from E15 to E11.

Discussion

Auditory brainstem neurons of vertebrates fire phase-locked APs at high rates with remarkable fidelity. We show here that late-developing NM neurons fire reliable APs to square-pulse current injections up to 200 Hz. In addition to the recognized role of K_{HVA} channels in this process, we also report that I_{NaR} of Na_V channels is an equally important component that operates synergistically with K_{HVA} channels to enable rapid AP firing in NM, an evolutionarily conserved process between birds and mammals likely promoting similar hearing functions. To our surprise, small I_{NaR} responses were present during a prehearing period (E11–12). At hearing onset (E14–16), I_{NaR} properties closely resemble late-developing NM neurons (E19–21), despite developmental refinement in Na_V channel protein expression patterns. In line with these results, NM neurons at E14–16 showed comparable frequency–firing ability to their late-developing counterparts, whereas NM neurons at E11–12 are most responsive to lower-frequency stimulations.

Factors regulating AP firing patterns in NM

K_{HVA} channels are a common regulator of AP kinetics (Rudy & McBain, 2001; Johnston *et al.* 2010). In the auditory brainstem of both birds and mammals, K_V3-containing channels are abundantly expressed (Wang *et al.* 1998; Parameshwaran *et al.* 2001; Parameshwaran-Iyer *et al.* 2003). Blockade or knockout of K_V3 channels results in wider APs that undermine the ability to generate APs at high rates (Wang *et al.* 1998; Klug & Trussell, 2006). We report a similar result here (Fig. 2). In addition, a recent study on *Xenopus* oocytes shows that $K_V3.1$ sub-units are able to produce resurgent potassium current
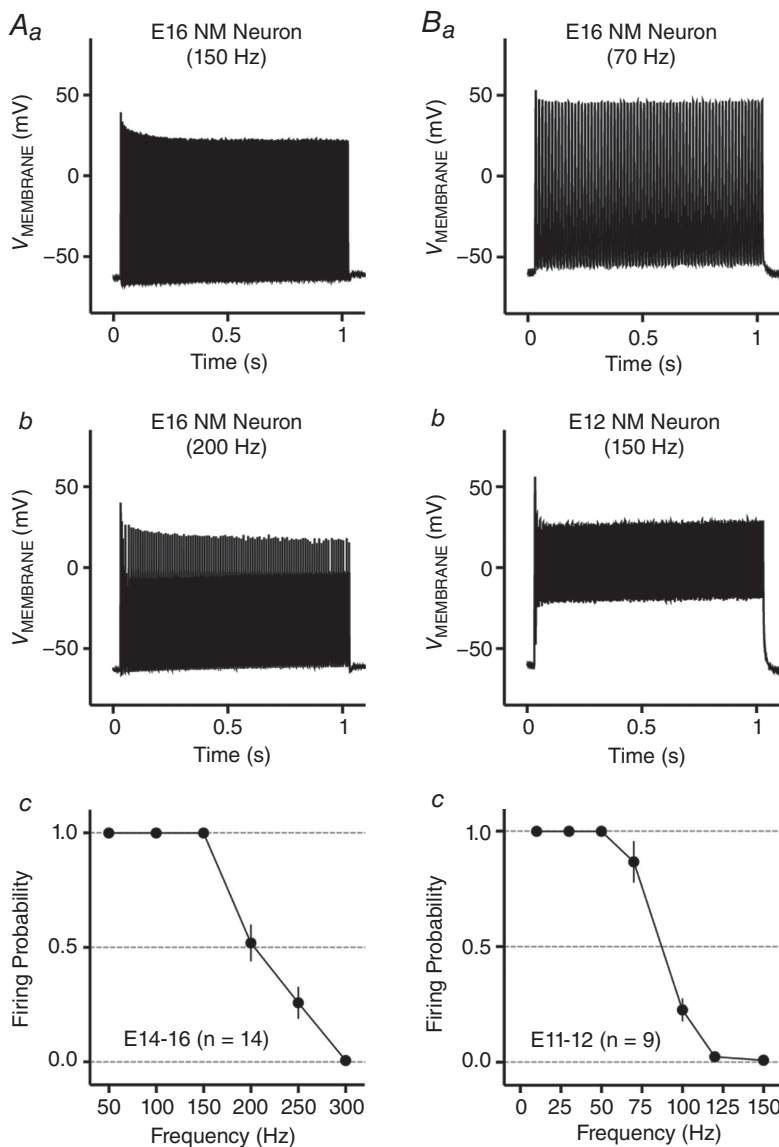

Figure 10. Frequency–firing pattern of NM neurons at E14–16 and E11–12
Aa and *b*, representative voltage responses recorded from an E16 NM neuron to current injections of square pulse trains at 150 and 200 Hz, respectively. *Ac*, population data showing firing probability of E14–16 NM neurons as a function of square pulse frequency. The strength of square pulse trains is 1 nA with a duration of 1 s. Individual square pulse width is 2 ms. *Ba* and *b*, representative voltage responses recorded from an E12 NM neuron to current injections of square pulse trains at 70 Hz and 150 Hz, respectively. *Bc*, population data showing firing probability of E11–12 NM neurons as a function of square pulse frequency. The strength of square pulse trains is 1 nA with a duration of 1 s. Individual square pulse width is 5 ms. Error bar, SEM.

during repolarization, which provides an additional repolarizing drive to the membrane (Labro *et al.* 2015). This property is not due to the open channel blocker but to the unique gating kinetics of $K_V3.1$ subunits, and it facilitates the termination of APs and thus likely promotes high-frequency repetitive firing. Nevertheless, it should be noted that 1 mM TEA used in the current study can also block a small portion of K_V7-containing channels and calcium-activated BK channels (Johnston *et al.* 2010). K_V7-containing channels are one of the K_{LVA} channels with slow activation kinetics (Johnston *et al.* 2010). They contribute minimally in NM and their immunoreactivity is minimal compared to K_V3 and K_V1 (Kuba *et al.* 2015). Due to their weak expression, blockade of K_V7-containing channels in NM neurons does not induce significant changes in AP properties (Kuba *et al.* 2015). In contrast, BK channels play an important role in regulating AP kinetics in many other neurons (Kimm *et al.* 2015). However, a previous study in NM reported no change in K_V current when external calcium was replaced by cobalt ions, suggesting minimal contribution of calcium-activated potassium current to the total current (Koyano *et al.* 1996). Therefore, K_V3-containing channels are probably the primary targets of 1 mM TEA applied in our experiments.
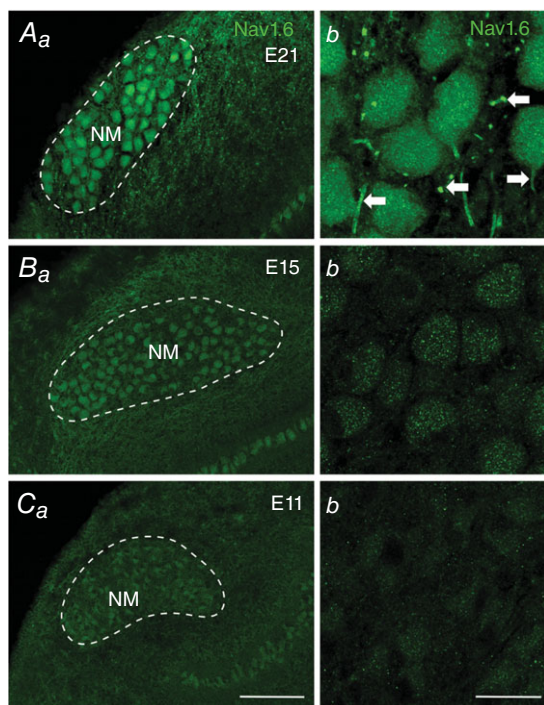
Figure 11. Na_V1.6 distribution in developing NM
Na_V1.6 immunoreactivity at E21 (*A*), E15 (*B*) and E11 (*C*). Left (*Aa*, *Ba* and *Ca*) and right (*Ab*, *Bb* and *Cb*) columns are low- and high-magnification confocal images, respectively. Dashed lines indicate the boundary of NM. NM, nucleus magnocellularis. Scale bars: 50 μm in *Ca* (left column), 10 μm in *Cb* (right column).

Another factor that regulates AP firing pattern is fast inactivation kinetics of Na_V channels (i.e. the steep decay slope of I_{NaT}) observed in auditory brainstem neurons (Ming & Wang, 2003; Hong *et al.* 2016). As demonstrated by double-pulse experiments, a second I_{NaT} can fully recover within 5 ms following the initial pulse (Leao *et al.* 2005; unpublished observation in NM), which explains in the current study why NM neurons are able to reliably follow the stimulus frequency at 150 Hz (interspike interval = 6.7 ms, Fig. 2*D*) after blockade of K_{HVA} channels. Finally, K_{LVA} channels with fast activation kinetics, such as K_V1-containing channels, work as another regulator of AP firing by controlling the time constant of passive membrane properties, shaping the speed of membrane voltage changes (Klug & Trussell, 2006).

I_{NaR} is an additional factor in regulating AP firing rates of NM neurons. The open channel block promotes Na_V channel availability and recovery immediately after brief depolarization in NM, a result consistent with previous studies (Raman & Bean, 2001; Patel *et al.* 2015). However, we report two major differences. First, Na_V channel availability is much higher in our study at any given recovery time period (Fig. 5*C*). This is likely because our recordings were made from intact neurons in brainstem slices that have significantly more neuron-specific Na_V channels. Previously reported data were obtained from the soma of dissociated Purkinje cells or from HEK cells transfected with Na_V channels. Second, the distinction in recovery time constant between the open channel block and classic inactivation state is smaller in our study (~1 ms *versus* > 5 ms, Fig. 5*D*). This may be attributed to relatively fast kinetics of I_{NaT} in auditory brainstem neurons. However, the extent to which the open channel block or the classic inactivation gate contributes to rapid I_{NaT} kinetics in NM is unclear.

'Real-time' I_{NaR} appears to be a relatively small inward Na_V current during repolarization from an initial I_{NaT}, as shown by our model NM neuron (Fig. 7*Ad*). This observation closely resembles experimental data when AP waveforms are used as voltage commands and the dynamic changes in Na_V current are documented (i.e. AP-clamp method; Raman & Bean, 1997, 1999). As seen from studies that utilized this technique, the I_{NaR} provided a small depolarizing drive immediately after an AP, important for subsequent AP firing (Raman & Bean, 1997). However, AP-clamp is susceptible to various technical limitations (e.g. space clamp errors), and as a result the majority of these studies were conducted on dissociated neurons (Raman & Bean, 1997; Do & Bean, 2003). Nevertheless, there are successful slice recordings with AP clamp from adendritic mesencephalic trigeminal neurons (Enomoto *et al.* 2006) Given the fact that the majority of late-developing NM neurons are also adendritic, AP-clamp experiments could provide valuable insight into the biological relevance of I_{NaR}. There are still

technical limitations (e.g. sample rate, kinetics, immature dendritic NM neurons, etc.) and therefore we employed a computational model to better address its functional significance. Indeed, removal of I_{NaR} reduced AP firing rate at 200 Hz for our model NM neuron (Fig. 7). Yet, the effects on Na$_V$ channels after the knockdown of open channel blocker remain to be determined, especially regarding the kinetics of I_{NaT} under experimental condition. These effects are dependent on the types of β-subunits expressed in NM neurons and their specific interactions with Na$_V$ α-subunits (Qu *et al.* 2001; Aman *et al.* 2009; Bant & Raman, 2010). Therefore, our computational model of NM neuron is subject to future improvements when more information about molecular substrates for the open channel blocker in NM is obtained.

Development of resurgent Na$_V$ current in NM

The inner ear of chickens only responds to loud sound (>80 dB) and afferent ganglion neurons present with poor frequency selectivity at E14–16 (Jones *et al.* 2006). It is surprising at this age that I_{NaR} properties are relatively established, except for decay kinetics, which are due in part to underdeveloped Na$_V$ α-subunit (Fig. 8, see below). I_{NaR} properties at E11–12 – a developmental period when the auditory system does not respond to sound and is considered 'prehearing' – differ greatly from those of the other age groups (Fig. 9). I_{NaR} development in NM parallels the development of frequency–firing pattern (Fig. 10), along with maturation of intrinsic AP properties and K$_V$ channel conductances as we previously reported (Hong *et al.* 2016). NM neurons at E14–16 generate APs as fast and reliably as late-developing neurons. Additionally, properties of K$_{LVA}$ and K$_{HVA}$ currents are underdeveloped at E11–12 but become more mature-like around hearing onset. Taken together, NM neurons have near-mature ion channel properties around hearing onset, suggesting a priming period during hearing development for establishing mature auditory functions.

I_{NaR} at E11–12, though small, may be important for shaping NM's AP firing pattern. In response to low-frequency (5–10 Hz) sinusoidal current injections, NM neurons at this age generate short bursts of APs per cycle, despite the fact that their overall low K$_V$ channel conductances are not sufficient to work against the largely depolarized membrane voltage during bursts (Hong *et al.* 2016). I_{NaR} also contributes to burst firing in other non-auditory neurons (Enomoto *et al.* 2006, 2007). We speculate that I_{NaR} at E11–12, albeit reduced, helps generate burst firing for immature NM neurons, but its functional significance at this age is unclear.

Anatomically, we detected strong Na$_V$1.6 expression at a late-developing stage (E21), which was dramatically reduced at hearing onset (E14–16) and prehearing (E11–12) periods (Fig. 11). Additionally, the majority of Na$_V$1.6 channels in late-developing neurons are located along the axons, while this distribution pattern is not evident for the other age groups. The Na$_V$1.6-positive punctate segments in late-developing NM neurons are likely to be the AIS and the nodes of Ranvier, respectively, though future immunocytochemistry with double staining of ankyrin G, a scaffold protein that marks the AIS, is needed to confirm this speculation (Kuba *et al.* 2014). The presence of I_{NaR} at E11–16 suggests that additional Na$_V$ subtypes may contribute to I_{NaR} during development of NM neurons. The following evidence supports this suggestion. First, strong expression of Na$_V$1.2 channels is observed at E11–15 in NM's postsynaptic target nuclei (i.e. nucleus laminaris) (Kuba *et al.* 2014). Second, studies in spinal sensory neurons report the generation of I_{NaR} from different Na$_V$ subtypes, including Na$_V$1.2 channels (Rush *et al.* 2005; Jarecki *et al.* 2010).

Resurgent Na$_V$ current is conserved across species and structures

I_{NaR} has been reported as a conserved property in numerous neuronal types in the mammalian cerebellum, cortex, brainstem and spinal cord (Afshari *et al.* 2004; Cummins *et al.* 2009; Lewis & Raman, 2014). As for the mammalian auditory system, I_{NaR} has been found at the calyx of Held and its postsynaptic target – the medial nucleus of trapezoid body (Leao *et al.* 2005; Kim *et al.* 2010). The only report of I_{NaR} beyond the scope of mammals comes from chicken Purkinje cells (Lewis & Raman, 2011). Our results from the current
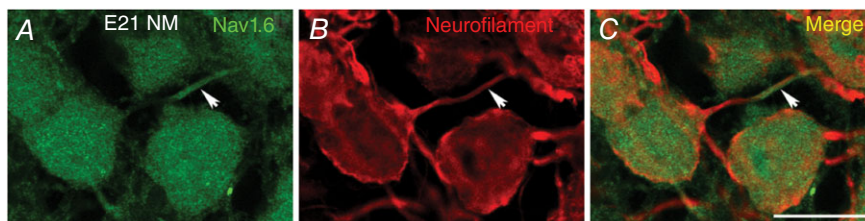
Figure 12. Axonal localization of Na$_V$1.6 immunoreactivity at E21
Double staining of Na$_V$1.6 and neurofilament in E21 NM. Arrows indicate a distinct segment containing Na$_V$1.6, which overlaps with neurofilament-stained axon that can be traced back to the cell body. NM, nucleus magnocellularis. Scale bars: 20 μm for all panels.

study further confirm its contribution in the chicken auditory brainstem. Here, the AP firing pattern of NM neurons (and the analogous bushy cells of the mammalian anteroventral cochlear nucleus) is essential for the encoding of behaviourally relevant acoustic cues. Central to this are established and specialized structural and functional features shared across species (Carr & Soares, 2002; Koppl, 2009; Grothe *et al.* 2010). The report of I_{NaR} in the current study strongly suggests yet another physiological feature shared across species within the central nervous system.

Despite the distribution of I_{NaR} in the central nervous system (Lewis & Raman, 2014), its underlying molecular substrates are unclear. The Na$_V$ β4-subunit has been identified as one important open channel blocker in cerebellar Purkinje cells, granule cells and dorsal root ganglia neurons (Grieco *et al.* 2005; Bant & Raman, 2010; Barbosa *et al.* 2015). Interestingly, the amino acid sequence of the β4-subunit is also conserved across species, from frogs to mammals, raising the possibility of its being the open channel blocker for avian NM neurons (Lewis & Raman, 2011). Nevertheless, questions are raised of whether the β4-subunit is the only possible open channel blocker. For example, both perirhinal and entorhinal pyramidal neurons show robust I_{NaR} but not β4 expression at high levels, possibly indicating multiple molecular substrates of I_{NaR} (Castelli *et al.* 2007; Nigro *et al.* 2012). In addition, FGF14, an intracellular protein and a member of the fibroblast growth factor homologous factors (FHFs), has been proposed as another key player in open channel block in Purkinje cells (Yan *et al.* 2014). A recent study on dorsal root ganglia neurons demonstrated that another member of the FHF family, FHF2, plays an important regulatory role for I_{NaR} (Barbosa *et al.* 2017). Interestingly, two isoforms of FHF2 have opposite effects on the amplitude of I_{NaR}. As for NM neurons, it should be noted that differences in I_{NaR} across development, especially at E11–12, might be attributed not only to different expression of Na$_V$ α-subunits, but also to changes in the open channel blocker molecular substrates themselves. Therefore, what the underlying open channel blockers for NM neurons are and how the developmental expression of these blockers shapes I_{NaR} maturation are interesting questions for future studies.

References

Afshari FS, Ptak K, Khaliq ZM, Grieco TM, Slater NT, McCrimmon DR & Raman IM (2004). Resurgent Na currents in four classes of neurons of the cerebellum. *J Neurophysiol* **92**, 2831–2843.

Akemann W & Knopfel T (2006). Interaction of Kv3 potassium channels and resurgent sodium current influences the rate of spontaneous firing of Purkinje neurons. *J Neurosci* **26**, 4602–4612.

Aman TK, Grieco-Calub TM, Chen C, Rusconi R, Slat EA, Isom LL & Raman IM (2009). Regulation of persistent Na current by interactions between beta subunits of voltage-gated Na channels. *J Neurosci* **29**, 2027–2042.

Anderson S, Skoe E, Chandrasekaran B & Kraus N (2010). Neural timing is linked to speech perception in noise. *J Neurosci* **30**, 4922–4926.

Bant JS & Raman IM (2010). Control of transient, resurgent, and persistent current by open-channel block by Na channel β4 in cultured cerebellar granule neurons. *Proc Natl Acad Sci USA* **107**, 12357–12362.

Barbosa C, Tan ZY, Wang R, Xie W, Strong JA, Patel RR, Vasko MR, Zhang JM & Cummins TR (2015). Navβ4 regulates fast resurgent sodium currents and excitability in sensory neurons. *Mol Pain* **11**, 60.

Barbosa C, Xiao Y, Johnson AJ, Xie W, Strong JA, Zhang JM & Cummins TR (2017). FHF2 isoforms differentially regulate Nav1.6-mediated resurgent sodium currents in dorsal root ganglion neurons. *Pflugers Archiv* **469**, 195–212.

Carr CE & Soares D (2002). Evolutionary convergence and shared computational principles in the auditory system. *Brain Behav Evol* **59**, 294–311.

Castelli L, Biella G, Toselli M & Magistretti J (2007). Resurgent Na$^+$ current in pyramidal neurones of rat perirhinal cortex: axonal location of channels and contribution to depolarizing drive during repetitive firing. *J Physiol* **582**, 1179–1193.

Cummins TR, Rush AM, Estacion M, Dib-Hajj SD & Waxman SG (2009). Voltage-clamp and current-clamp recordings from mammalian DRG neurons. *Nat Protoc* **4**, 1103–1112.

Do MT & Bean BP (2003). Subthreshold sodium currents and pacemaking of subthalamic neurons: modulation by slow inactivation. *Neuron* **39**, 109–120.

Eijkelkamp N, Linley JE, Baker MD, Minett MS, Cregg R, Werdehausen R, Rugiero F & Wood JN (2012). Neurological perspectives on voltage-gated sodium channels. *Brain* **135**, 2585–2612.

Enomoto A, Han JM, Hsiao CF & Chandler SH (2007). Sodium currents in mesencephalic trigeminal neurons from Nav1.6 null mice. *J Neurophysiol* **98**, 710–719.

Enomoto A, Han JM, Hsiao CF, Wu N & Chandler SH (2006). Participation of sodium currents in burst generation and control of membrane excitability in mesencephalic trigeminal neurons. *J Neurosci* **26**, 3412–3422.

Gao H & Lu Y (2008). Early development of intrinsic and synaptic properties of chicken nucleus laminaris neurons. *Neuroscience* **153**, 131–143.

Grieco TM, Malhotra JD, Chen C, Isom LL & Raman IM (2005). Open-channel block by the cytoplasmic tail of sodium channel β4 as a mechanism for resurgent sodium current. *Neuron* **45**, 233–244.

Grothe B, Pecka M & McAlpine D (2010). Mechanisms of sound localization in mammals. *Physiol Rev* **90**, 983–1012.

Grundy D (2015). Principles and standards for reporting animal experiments in *The Journal of Physiology* and *Experimental Physiology*. *Exp Physiol* **100**, 755–758.

Hines ML & Carnevale NT (1997). The NEURON simulation environment. *Neural Comput* **9**, 1179–1209.

Hong H, Rollman L, Feinstein B & Sanchez JT (2016). Developmental profile of ion channel specializations in the avian nucleus magnocellularis. *Front Cell Neurosci* **10**, 80.

Howard MA & Rubel EW (2010). Dynamic spike thresholds during synaptic integration preserve and enhance temporal response properties in the avian cochlear nucleus. *J Neurosci* **30**, 12063–12074.

Jarecki BW, Piekarz AD, Jackson JO 2nd & Cummins TR (2010). Human voltage-gated sodium channel mutations that cause inherited neuronal and muscle channelopathies increase resurgent sodium currents. *J Clin Invest* **120**, 369–378.

Jhaveri S & Morest DK (1982*a*). Sequential alterations of neuronal architecture in nucleus magnocellularis of the developing chicken: a Golgi study. *Neuroscience* **7**, 837–853.

Jhaveri S & Morest DK (1982*b*). Neuronal architecture in nucleus magnocellularis of the chicken auditory system with observations on nucleus laminaris: a light and electron microscope study. *Neuroscience* **7**, 809–836.

Johnston J, Forsythe ID & Kopp-Scheinpflug C (2010). Going native: voltage-gated potassium channels controlling neuronal excitability. *J Physiol* **588**, 3187–3200.

Jones TA & Jones SM (2000). Spontaneous activity in the statoacoustic ganglion of the chicken embryo. *J Neurophysiol* **83**, 1452–1468.

Jones TA, Jones SM & Paggett KC (2006). Emergence of hearing in the chicken embryo. *J Neurophysiol* **96**, 128–141.

Khaliq ZM, Gouwens NW & Raman IM (2003). The contribution of resurgent sodium current to high-frequency firing in Purkinje neurons: an experimental and modeling study. *J Neurosci* **23**, 4899–4912.

Kim JH, Kushmerick C & von Gersdorff H (2010). Presynaptic resurgent Na$^+$ currents sculpt the action potential waveform and increase firing reliability at a CNS nerve terminal. *J Neurosci* **30**, 15479–15490.

Kimm T, Khaliq ZM & Bean BP (2015). Differential regulation of action potential shape and burst-frequency firing by BK and Kv2 channels in substantia nigra dopaminergic neurons. *J Neurosci* **35**, 16404–16417.

Klug A & Trussell LO (2006). Activation and deactivation of voltage-dependent K$^+$ channels during synaptically driven action potentials in the MNTB. *J Neurophysiol* **96**, 1547–1555.

Koppl C (2009). Evolution of sound localisation in land vertebrates. *Current biology* **19**, R635–639.

Koppl C & Carr CE (1997). Low-frequency pathway in the barn owl's auditory brainstem. *J Comp Neurol* **378**, 265–282.

Koyano K, Funabiki K & Ohmori H (1996). Voltage-gated ionic currents and their roles in timing coding in auditory neurons of the nucleus magnocellularis of the chick. *Neurosci Res* **26**, 29–45.

Kuba H, Adachi R & Ohmori H (2014). Activity-dependent and activity-independent development of the axon initial segment. *J Neurosci* **34**, 3443–3453.

Kuba H, Ishii TM & Ohmori H (2006). Axonal site of spike initiation enhances auditory coincidence detection. *Nature* **444**, 1069–1072.

Kuba H, Oichi Y & Ohmori H (2010). Presynaptic activity regulates Na$^+$ channel distribution at the axon initial segment. *Nature* **465**, 1075–1078.

Kuba H, Yamada R, Fukui I & Ohmori H (2005). Tonotopic specialization of auditory coincidence detection in nucleus laminaris of the chick. *J Neurosci* **25**, 1924–1934.

Kuba H, Yamada R, Ishiguro G & Adachi R (2015). Redistribution of Kv1 and Kv7 enhances neuronal excitability during structural axon initial segment plasticity. *Nat Commun* **6**, 8815.

Kushmerick C, Renden R & von Gersdorff H (2006). Physiological temperatures reduce the rate of vesicle pool depletion and short-term depression via an acceleration of vesicle recruitment. *J Neurosci* **26**, 1366–1377.

Labro AJ, Priest MF, Lacroix JJ, Snyders DJ & Bezanilla F (2015). Kv3.1 uses a timely resurgent K$^+$ current to secure action potential repolarization. *Nat Commun* **6**, 10173.

Leao RM, Kushmerick C, Pinaud R, Renden R, Li GL, Taschenberger H, Spirou G, Levinson SR & von Gersdorff H (2005). Presynaptic Na$^+$ channels: locus, development, and recovery from inactivation at a high-fidelity synapse. *J Neurosci* **25**, 3724–3738.

Leao RN, Naves MM, Leao KE & Walmsley B (2006). Altered sodium currents in auditory neurons of congenitally deaf mice. *Eur J Neurosci* **24**, 1137–1146.

Lewis AH & Raman IM (2011). Cross-species conservation of open-channel block by Na channel β4 peptides reveals structural features required for resurgent Na current. *J Neurosci* **31**, 11527–11536.

Lewis AH & Raman IM (2014). Resurgent current of voltage-gated Na$^+$ channels. *J Physiol* **592**, 4825–4838.

Lu T, Wade K, Hong H & Sanchez JT (2017). Ion channel mechanisms underlying frequency-firing patterns of the avian nucleus magnocellularis: a computational model. *Channels (Austin)* **11**, 444–458.

Magistretti J, Castelli L, Forti L & D'Angelo E (2006). Kinetic and functional analysis of transient, persistent and resurgent sodium currents in rat cerebellar granule cells *in situ*: an electrophysiological and modelling study. *J Physiol* **573**, 83–106.

Ming G & Wang LY (2003). Properties of voltage-gated sodium channels in developing auditory neurons of the mouse in vitro. *Chin Med Sci J* **18**, 67–74.

Nigro MJ, Quattrocolo G & Magistretti J (2012). Distinct developmental patterns in the expression of transient, persistent, and resurgent Na$^+$ currents in entorhinal cortex layer-II neurons. *Brain Res* **1463**, 30–41.

Oertel D (1997). Encoding of timing in the brain stem auditory nuclei of vertebrates. *Neuron* **19**, 959–962.

Parameshwaran S, Carr CE & Perney TM (2001). Expression of the Kv3.1 potassium channel in the avian auditory brainstem. *J Neurosci* **21**, 485–494.

Parameshwaran-Iyer S, Carr CE & Perney TM (2003). Localization of KCNC1 (Kv3.1) potassium channel subunits in the avian auditory nucleus magnocellularis and nucleus laminaris during development. *J Neurobiol* **55**, 165–178.

Patel RR, Barbosa C, Xiao Y & Cummins TR (2015). Human Nav1.6 channels generate larger resurgent currents than human Nav1.1 channels, but the Navβ4 peptide does not protect either isoform from use-dependent reduction. *PLoS One* **10**, e0133485.

Qu Y, Curtis R, Lawson D, Gilbride K, Ge P, DiStefano PS, Silos-Santiago I, Catterall WA & Scheuer T (2001). Differential modulation of sodium channel gating and persistent sodium currents by the β1, β2, and β3 subunits. *Mol Cell Neurosci* **18**, 570–580.

Raman IM & Bean BP (1997). Resurgent sodium current and action potential formation in dissociated cerebellar Purkinje neurons. *J Neurosci* **17**, 4517–4526.

Raman IM & Bean BP (1999). Ionic currents underlying spontaneous action potentials in isolated cerebellar Purkinje neurons. *J Neurosci* **19**, 1663–1674.

Raman IM & Bean BP (2001). Inactivation and recovery of sodium currents in cerebellar Purkinje neurons: evidence for two mechanisms. *Biophys J* **80**, 729–737.

Rebillard G & Rubel EW (1981). Electrophysiological study of the maturation of auditory responses from the inner ear of the chick. *Brain Res* **229**, 15–23.

Rudy B & McBain CJ (2001). Kv3 channels: voltage-gated K$^+$ channels designed for high-frequency repetitive firing. *Trends Neurosci* **24**, 517–526.

Rush AM, Dib-Hajj SD & Waxman SG (2005). Electrophysiological properties of two axonal sodium channels, Nav1.2 and Nav1.6, expressed in mouse spinal sensory neurones. *J Physiol* **564**, 803–815.

Sanchez JT, Seidl AH, Rubel EW & Barria A (2011). Preparation and culture of chicken auditory brainstem slices. *J Vis Exp*, 2527.

Saunders JC, Coles RB & Gates GR (1973). The development of auditory evoked responses in the cochlea and cochlear nuclei of the chick. *Brain Res* **63**, 59–74.

Shannon RV, Zeng FG, Kamath V, Wygonski J & Ekelid M (1995). Speech recognition with primarily temporal cues. *Science* **270**, 303–304.

Trussell LO (1997). Cellular mechanisms for preservation of timing in central auditory pathways. *Curr Opin Neurobiol* **7**, 487–492.

Trussell LO (1999). Synaptic mechanisms for coding timing in auditory neurons. *Annu Rev Physiol* **61**, 477–496.

Wang LY, Gan L, Forsythe ID & Kaczmarek LK (1998). Contribution of the Kv3.1 potassium channel to high-frequency firing in mouse auditory neurones. *J Physiol* **509**, 183–194.

Wang LY & Kaczmarek LK (1998). High-frequency firing helps replenish the readily releasable pool of synaptic vesicles. *Nature* **394**, 384–388.

Warchol ME & Dallos P (1990). Neural coding in the chick cochlear nucleus. *J Comp Physiol A* **166**, 721–734.

Yan H, Pablo JL, Wang C & Pitt GS (2014). FGF14 modulates resurgent sodium current in mouse cerebellar Purkinje neurons. *Elife* **3**, e04193.

Additional information

Competing interests

The authors declare no competing financial interests.

Author contributions

All authors have approved the final version of the manuscript and agree to be accountable for all aspects of the work. All persons designated as authors qualify for authorship, and all those who qualify for authorship are listed. HH, TL, XW, YW and JTS designed the study. HH performed electrophysiology experiments at Northwestern University. TL performed computational modeling experiments at Northwestern University. XW and YW performed immunocytochemical experiments at Florida State University. HH, TL, XW, YW and JTS analyzed/interpreted data and wrote the manuscript.

Funding

Acknowledgements